# Towards a Plastic Neuronal Signal Sensor

Experiments on the suitability of organic dual-gate field-effect transistors for use in future sensors to detect and measure neuronal signals

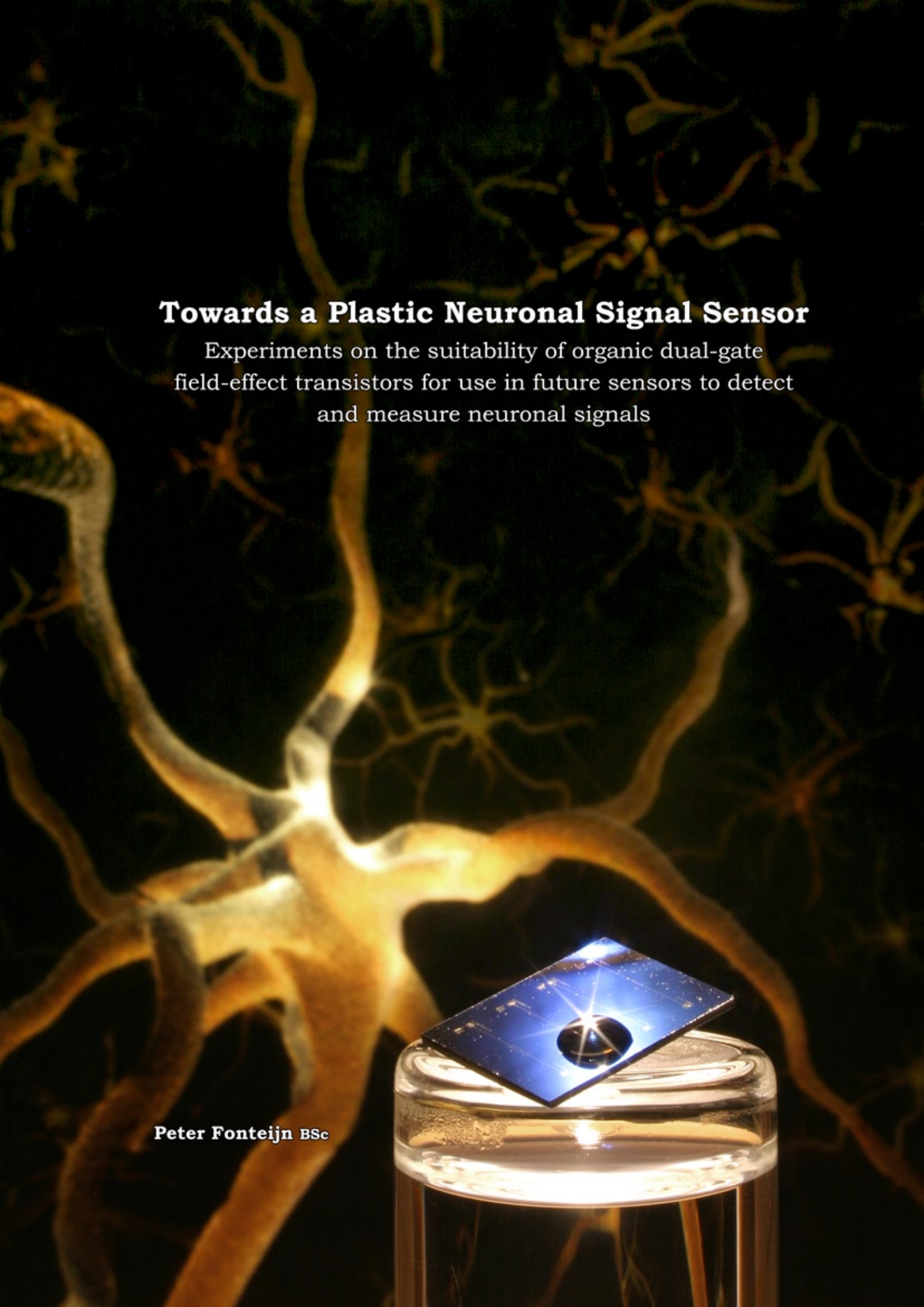

**Peter Fonteijn** BSc

# Towards a Plastic Neuronal Signal Sensor

Experiments on the suitability of organic dual-gate field-effect transistors for use in future sensors to detect and measure neuronal signals

**Peter Fonteijn BSc**

Supervised by
Ir. J.J. Brondijk
Prof. Dr. B. de Boer
Prof. Dr. Ir. P.W.M. Blom

*Molecular Electronics - Physics of Organic Semiconductors*
*Zernike Institute for Advanced Materials*
*Faculty of Mathematics and Natural Sciences*
*University of Groningen*

university of groningen / faculty of mathematics and natural sciences / zernike institute for advanced materials

een beetje voor opa (†1994)

The work described in this report was carried out between September 2007 and July 2008 as part of the Top Master Programme in Nanoscience and was performed in the research group Molecular Electronics - Physics of Organic Semiconductors, part of the Zernike Institute for Advanced Materials, at the University of Groningen.

# Preface

It is about eleven months ago now that I started my master research project in the group Molecular Electronics - Physics of Organic Semiconductors. After the pretty tough first year of the Nanoscience top master, the research project seemed to become much more relaxing. And indeed, this year was not as heavy as before, but still not everything was easygoing.
Being a chemist, truly understanding the physical properties of materials have not always been simple. The ease with which the physicist juggled with formulas, interpreted current-voltage graphs and explained the behaviour of the materials took some time to understand and, eventually, to do myself as well. I hope I succeeded a bit in this.
I have to thank some people that helped, supported or supervised me. First of all, of course, Paul Blom and Bert de Boer for giving me the opportunity to do this project and for giving me the freedom to push things in a direction I was interested in. Many thanks to Johan for introducing me in the cleanroom and in the wondrous world of current measurements, and also for listening to and answering all my questions and ideas. Also some words of thanks to Stijn, Xiaoran and Ilias for the nice discussions, talks and chats, which were not only about research usually.
Time flies when you are playing around in the lab and in the cleanroom. I would have liked to do many more things, although this was impossible in only one year. Nevertheless, the most important experiments have been carried out during the research project and eventually have been described in this thesis. The first two chapters give an overview of some important theory involved. Next, the experiments are described and finally all results are presented and discussed. Hopefully, the obtained results will form a basis for further experiments and research projects.
For all people that were scared by the title of this thesis, but are still wondering what I did this year, take a look at the very last “Euhh, wát heb je gedaan?!” chapter (Euhh, whát did you do?!). It might give you some idea on what I spent my time the last few months.

# Voorwoord

Het is nu bijna elf maanden geleden dat ik met mijn master onderzoeksproject begon in de groep Molecular Electronics - Physics of Organic Semiconductors. Na het vrij zware eerste jaar van de Nanoscience top master leek het onderzoeksproject een stuk relaxter te worden. En inderdaad, het afgelopen jaar was lang niet zo heftig als daarvoor, hoewel nog steeds niet alles zomaar vanzelf ging.
Als chemicus was het niet altijd even gemakkelijk om de fysische eigenschappen van materialen volledig te begrijpen. Het gemak waarmee fysici met formules goochelden, stroom-voltage grafieken interpreteerden en het gedrag van materialen verklaarden,

kostte aardig wat tijd om te begrijpen en, uiteindelijk, ook zelf toe te passen. Hopelijk ben ik hier een beetje in geslaagd.
Ik wil een aantal mensen bedanken die mij geholpen, ondersteund of begeleid hebben. In de eerste plaats natuurlijk Paul Blom en Bert de Boer, die mij de mogelijkheid gaven dit onderzoeksproject uit te voeren en die me de vrijheid gaven een richting in te gaan waarin ik geïnteresseerd was. Veel dank aan Johan voor de introductie in de cleanroom en in de wondere wereld van de stroommetingen en ook voor het luisteren naar en beantwoorden van al mijn vragen en ideeën. Ook dank aan Stijn, Xiaoran en Ilias voor de leuke discussies, gesprekken en praatjes, die meestal niet alleen maar over onderzoek gingen.
De tijd vliegt voorbij als je in het lab en in de cleanroom aan het prutsen bent. Ik had graag veel meer dingen gedaan, hoewel dit onmogelijk was in één jaar. Niettemin zijn de belangrijkste experimenten uitgevoerd tijdens het onderzoeksproject en uiteindelijk in deze scriptie beschreven. De eerste twee hoofdstukken geven een overzicht van een belangrijk stuk theorie. Daarna worden de experimenten beschreven en uiteindelijk worden alle resultaten getoond en bediscussieerd. Hopelijk vormen de behaalde resultaten een basis voor verdere experimenten en onderzoeksprojecten.
Voor wie werd afgeschrikt door de titel van deze scriptie, maar toch benieuwd is naar wat ik dit jaar gedaan heb, kijk even naar het laatste “Euhh, wát heb je gedaan?!” hoofdstuk. Het zal je een idee geven waaraan ik de laatste paar maanden mijn tijd heb besteed.

Peter Fonteijn

Groningen, July/Juli 2008

# Abstract

Detecting and measuring neuronal signals is essential for neural prostheses, but it is also of interest for studying neurons and neuronal activity in general. Much research has been carried out into new materials and sensors suitable for interfacing the nervous system. A first step towards a new type of sensor to detect and measure neuronal signals, based on polymeric dual-gate field-effect transistors, is presented here. Different combinations of semiconducting and insulating organic polymers have been studied for their dual-gate field-effect transistor characteristics. Transistors composed of PAA (semiconductor) and PMMA (top insulator) were the most suitable transistors so far to eventually be used in a sensor. Two active channels were present in the semiconductor layer and the threshold voltage could be accurately controlled by the second gate electrode. Many experiments have been carried out in order to obtain water blocking insulator layers to avoid contact between water and the transistor electrodes. PMMA was water blocking when its thickness was at least 1000 nm. Adding a crosslinker decreased this lower limit down to 500 nm, but led to doping of PAA with HCl. P4VP was used as an HCl scavenger and -blocking layer to avoid doping of PAA, which was successful to a certain extent. All studied insulator structures with P4VP, however, were not water blocking. The single-gate field-effect transistor characteristics of PAA, coated with PMMA, were not influenced by either water or solutions of NaCl or KCl. The aqueous environment essential for neurons to survive on top of a field-effect transistor is therefore not likely to cause any interference with the transistor. All results together show the suitability of the studied transistors for use in neuronal signal sensors.

# Contents

# 1. Introduction

One of the most important organ systems in humans, and animals in general, is the nervous system. The nervous system is a complex and specialized network that regulates all aspects of bodily function. It can be considered as a highly advanced electrical wiring system capable of transporting and processing a wide variety of information and directing many different processes.
For centuries, people have been fascinated by the nervous system and soon one understood its connection with movement and sensation. From a scientific viewpoint, understanding the principles behind the nervous system and the mechanisms involved, was for a long time, and still is, a key focus of research. When knowledge grew, connections with diseases, physical problems and disabilities were established. Nowadays, researchers try not only to understand the nervous system even better, but also to employ their understanding in practical applications from the application viewpoint. In the end, one hopes to cure patients from diseases related to the nervous system and to improve the lives of people with physical problems or disabilities.

Worldwide hundreds of thousands of people suffer from neurological injuries and diseases.[1] In many cases, these diseases and injuries lead to loss of function in specific parts of the body. A well-known example is paralysis of the limbs due to spinal cord lesion. In some cases the disability is so severe that it not only precludes mobility, but also prevents patients from feeding themselves or verbally communicating in a meaningful way.
Prostheses can be of grateful help for people suffering from (neurological) disabilities. If it is possible to detect and measure the neuronal signals from the part of the nervous system that is still intact and working properly, these signals can be interpreted and translated into commands for controlling the prostheses.[2] In the same way it can also provide patients with a means of communication by interacting with a computer. In the end, it might even give back patients the control over their own paralyzed limb, ideally with a feedback system to receive sensory signals from the limb.

This field of neural prosthetics, to help restore function in the nervous system, is a very large field. It includes many different disciplines all working on different elements or applications. All neural prostheses have in common that they have to interface with the nervous system to detect and measure the neuronal signals. Originally non-invasive techniques were used,[2,3] like measuring signals from the skin. Invasive, electrode-based sensor techniques, however, are more attractive, since they offer high signal quality[3] and the ability to detect and measure signals from individual neurons.[1] Therefore, they have the resolution needed to control a prosthetic limb in real time.[4] Examples range from cuff electrode-based sensors[5] to silicon- and ceramic microelectrode arrays.[4] Although more attractive, implantable electrode-based sensors are only suitable if they are biocompatible. Obviously, the materials in

these sensors cannot be toxic, but also the response of tissue on the implants is important.[4] Inflammation and scar formation should be avoided as much as possible, also in order to prevent loss of signal quality over time.

Research is still carried out into new materials and sensors suitable for interfacing the nervous system. A first step towards a new type of sensor to detect and measure neuronal signals is presented here. Based on a field-effect transistor geometry, this sensor will be a small and sensitive device. The use of proper organic materials increases its biocompatibility, making this sensor a promising neural interface and a future candidate for integration into neural prostheses.
The work described here is related to a four-year research project that is part of a European project on “Sensing BIOsystems and their Dynamics in fluids with Organic Transistors” (BIODOT). In this work a first step towards a functioning neuronal sensor has been made, focussing on transistor characteristics, blocking of water and influence of salt solutions. The results show the suitability of the transistors for use in neuronal signal sensors.

# 2. Theoretical overview

This chapter gives a general overview of theory involved in neural interfacing. It provides essential background information on the working principles of neuronal signalling and it deals with detecting and measuring these signals. Also some work already done in the field is highlighted and related to the work described here. In the end, a short outline is given of the experiments done in this work.

## 2.1. Neuronal signalling

The nervous system is a complex and specialized network that provides for rapid communication between widely separated parts of the body. It regulates all aspects of bodily function, like governing reactions to stimuli, processing information and generating signals to control complex behaviour.[6] The nervous system is one of the most important organ systems and a major communication network in the body.

### 2.1.1. Neurons

In vertebrates, like humans, the nervous system is divided into the central nervous system and the peripheral nervous system.[7] The central nervous system, consisting of the brain and the spinal cord, is the main processing unit of the nervous system.[6] It is connected to the peripheral nervous system, the part of the nervous system in the rest of the body, through nerves. The major building blocks of nerves, and of the nervous system in general, are neurons. Neurons are electrically excitable cells that are capable of receiving, conducting and transmitting signals.[6] A neuron consists of a cell body with two main processes extending from it, the axon and the dendrites.[6,7] The cell body contains the nucleus of the cell and is the site of synthesis of all neuronal components.[7] The axon, a long single fibre, extends from the cell body and conducts signals away from it. The dendrites on the other hand receive signals and conduct them towards the cell body. A neuron typically contains multiple of these short branched dendrites, like antennae, to provide an enlarged surface area for receiving signals (see Figure 1). Also the end of the axon is branched into several so-called axon terminals. Signals are passed from these axon terminals to the dendrites of neighbouring neurons.[6,7] Since neurons connect the central nervous system with the rest of the body, axons can be very long. In humans, axons may be a meter or more in length with a diameter of only a few micrometers.[7]

The signals transmitted through a neuron are of electrical origin, allowing for very fast transmission along the neuron with a speed up to 100 m $s^{-1}$.[6,7] These signals are known as action potentials, or nerve impulses, and are travelling waves of electrical excitation.[6] The action potential finds its origin in changes of the membrane potential, an electrical potential across the membrane of the neuron.[6,7] Signals received by the dendrites, and also in some neurons by the cell body, cause electrical disturbances in the membrane potential. These received signals can either be of chemical origin, for

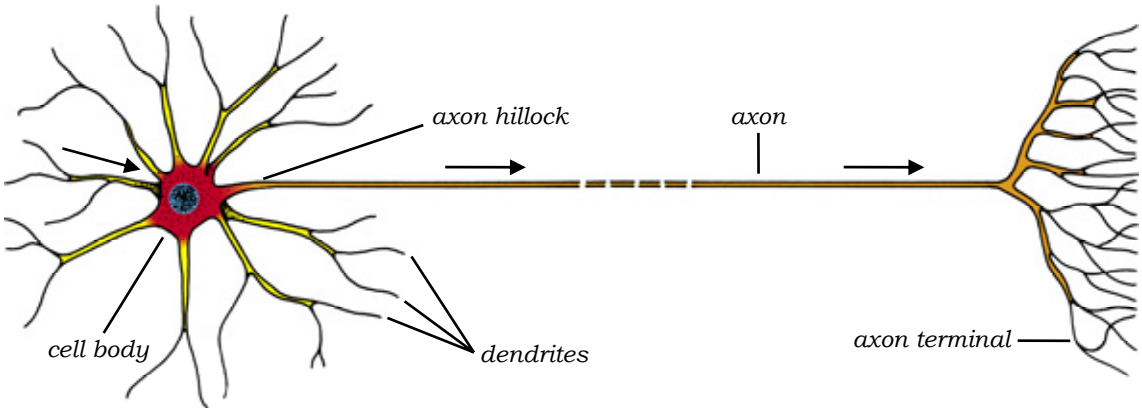


**Figure 1: Structure of a neuron.** *A schematic structure of a typical neuron, showing the dendrites (yellow), the cell body (red) with the nucleus (blue), the axon hillock, the axon (orange) and the axon terminals. Arrows indicate the direction of signal transmission. The length of an axon can range from less than 1 mm to more than 1 meter, with a typical diameter of a few micrometers. Adapted from Alberts.*[6]

example neurotransmitter molecules, or of electrical origin. The induced electrical disturbances spread to the axon hillock, the junction of the axon and the cell body. When the summation of all electrical disturbances that reach the axon hillock causes the magnitude of the membrane potential to drop below a threshold value, action potentials are generated.[7] These action potentials then run from the axon hillock to the axon terminals, in other words the neuron fires.

### 2.1.2. The membrane potential

Cells can be seen as little bags containing many different molecules related to replication, metabolic processes, transport mechanisms and so on. These molecules are dissolved in the cytosol, the internal cell fluid, and can not escape from the cell due to the surrounding semipermeable plasma membrane. Many of these molecules are (highly) charged at the pH retained in the cell. Therefore, they attract lots of extra inorganic ions of opposite charge from the outside through the membrane,[6] known as the Donnan effect.[8] The result is an uneven distribution of these ions among the inside and outside of the cell with the higher concentration at the inside. The Donnan effect, therefore, leads to a much higher osmolarity, the total number of dissolved particles, inside the cell than outside it. Any system, however, will try to reach a situation in which the osmolarity is the same everywhere. Since the membrane is highly permeable to water, osmosis takes place.[6] Osmosis is the movement of water molecules from a place with low osmolarity to a place with high osmolarity in order to reach the same osmolarity everywhere.[7] In the case of the cell, water will continuously flow into the cell, causing it to grow and eventually burst.[6]
To prevent itself from bursting, a cell actively pumps out inorganic ions until the osmolarity inside the cell is the same as that of the fluid surrounding the cell. When the osmolarity is the same on both sides of the membrane, no net water flows into or out of the cell.[6] Due to the active ion pumping, cells have a typical internal

**Table 1: Typical ion concentrations.** *Concentrations inside (intracellular) and outside (extracellular) a typical vertebrate neuron for sodium ($Na^+$) ions, potassium ($K^+$) ions and chloride ($Cl^-$) ions. $A^-$ indicates all negatively charged molecules that can not cross the semipermeable plasma membrane. A cell contains many more ions, neglected here owing to their low concentrations. Numbers adapted from Alberts[6] and Darnell[7].*

| | *Intracellular* | *Extracellular* |
|---|---|---|
| $Na^+$ | *12 mM* | *147 mM* |
| $K^+$ | *140 mM* | *5 mM* |
| $Cl^-$ | *4 mM* | *117 mM* |
| $A^-$ | *148 mM* | *35 mM* |

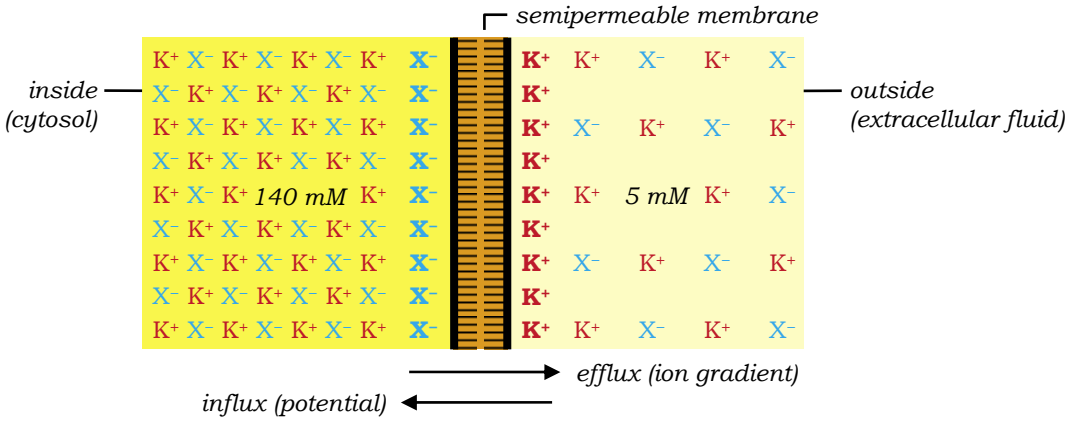


**Figure 2: $K^+$ Equilibrium membrane potential.** *A schematic drawing of the origin of the $K^+$ membrane potential. $K^+$ ions leave the cell down their concentration gradient. The negative charges left behind build up a potential, opposing the efflux of $K^+$ ions. When the net efflux of $K^+$ ions stops, this potential has reached the magnitude of the equilibrium membrane potential. $X^-$ denotes all negatively charged ions. Other ions have been omitted for clarity.*

environment with specific concentrations of inorganic ions (see Table 1). These ion concentrations are kept constant, not only to prevent the cell from bursting, but also since many metabolic processes are driven by or connected to these ions and their concentrations.[7]

Due to the typical internal environment, ion concentration differences are created between the inside and outside of the cell (see Table 1). The plasma membrane, however, contains many potassium leak channels, through which potassium ($K^+$) ions can freely move into our out of the cell. As a result of their high concentration inside the cell, $K^+$ ions therefore have a tendency to leave the cell down their concentration gradient. All $K^+$ ions that flow out of the cell leave behind a negative charge, as such building up a negative potential at the inside of the cell with respect to the outside, the so-called membrane potential. This membrane potential results in an electric field across the membrane, which tends to oppose the further efflux of $K^+$ ions (see

Figure 2). When the electric field reaches a value where its driving force exactly balances the effect of the concentration gradient, that is, when the electrochemical gradient is zero, the net efflux of $K^+$ ions stops. The charges that give rise to the membrane potential lie in a small layer of less than 1 nm at the inside of the membrane surface. They are held at the surface by the electrical attraction to the opposite charges on the outer side of the membrane.[6]

The magnitude of the equilibrium membrane potential established by the efflux of $K^+$ ions can be calculated by the (equilibrium) Nernst equation[9]

$$V = \frac{RT}{zF} \ln \frac{[\text{ion}]_{\text{out}}}{[\text{ion}]_{\text{in}}} \qquad (1)$$

where $V$ is the equilibrium membrane potential, $R$ is the gas constant (8.3145 J $mol^{-1}$ $K^{-1}$), $T$ is the temperature (around 310 K in cells), $z$ is the valence of the ions (+1 for $K^+$ ions), $F$ is the Faraday constant ($9.64853 \times 10^4$ C $mol^{-1}$), and $[\text{ion}]_{\text{out}}$ and $[\text{ion}]_{\text{in}}$ are the concentrations of the ions outside and inside the cell respectively. For a typical vertebrate neuron the equilibrium membrane potential due to the $K^+$ ions, therefore, is −89 mV, using the concentrations from Table 1.

Not only $K^+$ ions move across the membrane establishing a membrane potential. Also sodium ($Na^+$) ions and chloride ($Cl^-$) ions are involved in the creation of the membrane potential. The plasma membrane, however, does not show the same permeability for all three types of ions. When calculating the resultant membrane potential, this difference in permeability has to be taken into account. Therefore, the ion concentrations are weighted with their respective permeability constant $P$, a measure of the ease with which a certain ion crosses the membrane.[7] For monovalent ions the Nernst equation (Equation 1) now becomes

$$V = \frac{RT}{F} \ln \frac{\sum_{i^+} P_{i^+}[i^+]_{\text{out}} + \sum_{j^-} P_{j^-}[j^-]_{\text{in}}}{\sum_{i^+} P_{i^+}[i^+]_{\text{in}} + \sum_{j^-} P_{j^-}[j^-]_{\text{out}}} \qquad (2)$$

known as the Goldman-Hodgkin-Katz voltage equation after work of Goldman, and Hodgkin and Katz[10]. In this equation $i^+$ denotes the positive ions and $j^-$ denotes the negative ions. The signs of the ion valences have been taken into account by placing the inside negative ions in the numerator and the outside negative ions in the denominator. The Nernst equation (Equation 1) is a special case of this Goldman-Hodgkin-Katz voltage equation, only valid when just one type of ions is involved.[7]

Typical values of the permeability constants are $10^{-10}$ m $s^{-1}$, $10^{-9}$ m $s^{-1}$ and $10^{-10}$ m $s^{-1}$ for $Na^+$, $K^+$ and $Cl^-$ respectively.[7] Hence, using Equation 2, the resultant equilibrium membrane potential, or resting membrane potential, of a typical vertebrate neuron is around −54 mV. This potential is less negative than the $K^+$ equilibrium membrane potential. This is mainly due to the permeability of the membrane to $Na^+$ ions, which tends to make the membrane potential more positive.[7] Although −54 mV seems like a very low potential, it has to be taken into account that the plasma membrane is only about 5 nm thick. Therefore, the electric field across the membrane has a magnitude well over $10 \times 10^6$ V $m^{-1}$.

Changes in the permeability of the membrane to certain ions can drastically change the membrane potential. An increase of $P_K$, the permeability constant for $K^+$, results in

extra efflux of $K^+$ ions down their concentration gradient. Therefore, the membrane potential becomes more negative (hyperpolarization), approaching the $K^+$ equilibrium membrane potential, $V_K$, of −89 mV. On the other hand, a decrease of $P_K$ results in less efflux of $K^+$ ions and therefore a less negative membrane potential (depolarization). Also an increase of $P_{Na}$ results in depolarization, due to extra influx of $Na^+$ ions down their concentration gradient. If the increase of $P_{Na}$ is large enough, the membrane potential can even become positive, approaching $V_{Na}$ (+67 mV). A decrease of $P_{Na}$ on the other hand results in hyperpolarization again. Also an increase of $P_{Cl}$ gives rise to hyperpolarization. The extra influx of $Cl^-$ ions leads to a membrane potential approaching $V_{Cl}$ (−90 mV). Conversely, a decrease of $P_{Cl}$ causes depolarization again.[7]

### 2.1.3. The action potential

The potential on the plasma membrane of most cells generally does not vary with time. Such cells are electrically inactive. In contrast, the membrane potential of neurons does undergo changes over time. These changes are the origin of the electrical signals transmitted through a neuron and are therefore central to the function of neurons.[7]

Signals received on a neuron may induce a sudden electrical disturbance at a single point along the membrane, leading to, for example, depolarization. The inside of the membrane now has a relative excess of positive ions at this point. The cytosol has a high conductivity for ions, so these positive ions will tend to move away from the initial depolarization site. In doing so, they depolarize the adjacent parts of the membrane. Since the transport is based on diffusion, this signal transmission is known as passive spread of signals. Some of the excess positive ions inside the cell will leak back across the membrane into the surroundings. As a result, the magnitude of depolarization decreases exponentially with increasing distance from the site of initial depolarization. Signals, therefore, can be transmitted by passive spread only over short distances, up to about 5 mm, which is enough for signal transmission in dendrites and the cell body.[6,7] Neurons with a very short axon also utilize passive spread in signal transmission.[7] The axon of most neurons is, however, much larger than 5 mm. Hence, passive spread of signals is insufficient to transmit signals all the way down to the axon terminals. To maintain a high magnitude of the signal, it has to be amplified actively. This amplified signal is known as the action potential.[6]

The generation of an action potential is directly related to the phenomena of depolarization and hyperpolarization, and therefore to the permeability of the membrane to different ions. The plasma membrane is able to change its permeability to certain ions by means of specific ion channels. These transmembrane channels are embedded in the plasma membrane and can be opened and closed to allow more or less ions to leak across the membrane. The channels involved in the generation of the action potential are all voltage-gated ion channels. This means that they open or close in response to the membrane potential. When the membrane becomes depolarized beyond a certain threshold value, voltage-gated $Na^+$ channels are opened and the permeability of the membrane to $Na^+$ ions increases. This results in an even larger depolarization, moving towards $V_{Na}$. The depolarization of the membrane also induces the opening of voltage-gated $K^+$ channels. These channels, however, open with a short delay and are therefore known as delayed $K^+$ channels. The opening of the delayed $K^+$

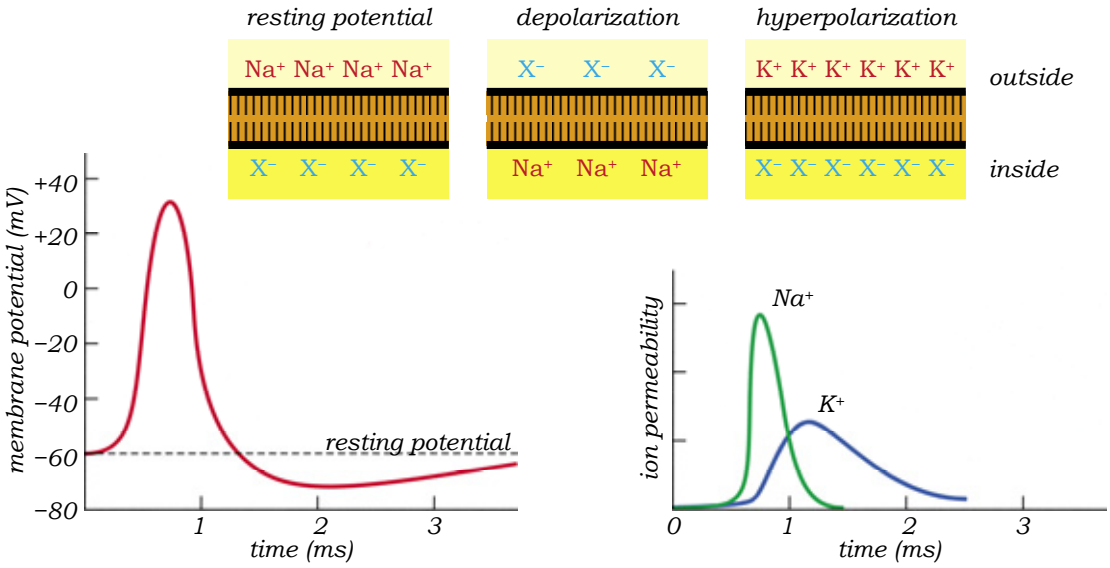


**Figure 3: Action potential and membrane permeability.** *Typical changes in membrane potential of a neuron after stimulation at t = 0 ms (left: red curve). First depolarization takes place, due to increased $Na^+$ permeability. Subsequently, the membrane potential decreases again, due to increased $K^+$ permeability. After closure of both the voltage-gated $Na^+$ and $K^+$ channels, the membrane potential gradually returns to its resting value (black dashed line). The corresponding typical change in ion permeability is depicted on the right for $Na^+$ (green curve) and $K^+$ (blue curve). The ions present at the inner- and outer surface of the membrane are schematically shown above the curves in the case of resting potential, depolarization and hyperpolarization. Only the major contributing ions, that is, $Na^+$, $K^+$ and the negatively charged ions $X^-$, are depicted. Curves adapted from Darnell.*[7]

channels increases the membrane permeability to $K^+$ ions, which results in hyperpolarization directly after the depolarization. The voltage-gated $Na^+$ channels immediately close after initial opening. The voltage-gated $K^+$ channels remain open as long as the membrane is depolarized. When both types of channels are closed again, the permeability of the membrane to $Na^+$ ions and $K^+$ ions returns to the original values. Gradually, the membrane potential repolarizes to the resting value (see Figure 3). This cycle of depolarization, hyperpolarization and repolarization lasts for only a few milliseconds. The short peak of extensive depolarization, and therefore amplified signal, is the actual action potential.[6,7]

Transmission of the action potential is connected to passive spread and the high conductivity of the cytosol. Due to the large influx of $Na^+$ ions after initial depolarization, some of the $Na^+$ ions will start to diffuse along the length of the axon. In doing so, adjacent parts of the membrane are depolarized beyond the threshold level for opening of voltage-gated $Na^+$ channels, inducing an action potential. This action potential again induces another action potential at the next site and so on, resulting in a travelling wave of electrical excitation. After initial opening, the $Na^+$ channels, however, remain in an inactivated closed state for a few milliseconds. In this inactivated state, the $Na^+$ channels can not open again, avoiding a new action

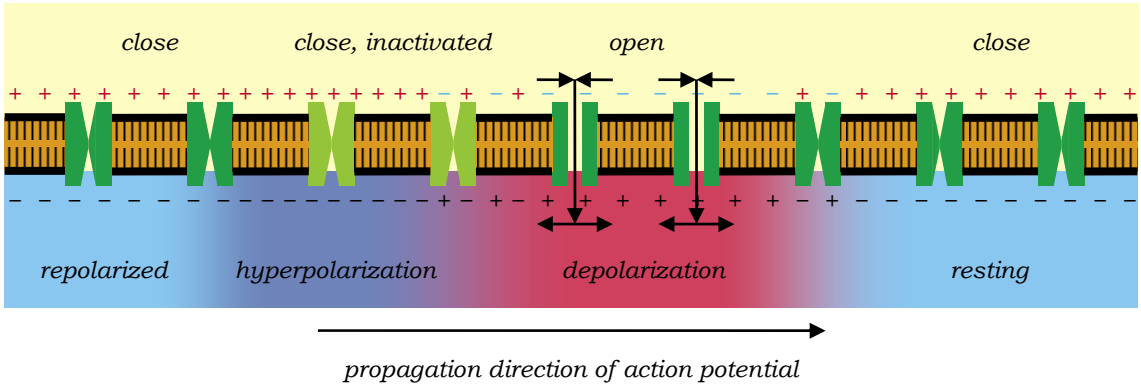


**Figure 4: Transmission of the action potential.** *Voltage-gated $Na^+$ channels open after initial depolarization. Influx of $Na^+$ ions depolarizes neighbouring sites. Only $Na^+$ channels in the forward direction will open due to this depolarization; the other $Na^+$ channels are inactivated. Therefore, action potentials are only transmitted in one direction. In this schematic illustration the voltage-gated $K^+$ channels have been omitted for clarity. Illustration after Alberts[6] and Darnell[7].*

potential to be generated. Therefore, action potentials can only be transmitted in the forward direction (see Figure 4). Due to the self-amplification of the depolarization, the diffusion of $Na^+$ ions and the inactivated $Na^+$ channels, signals are transmitted all along the axon from the axon hillock to the axon terminals.[6,7]

## 2.2. Detecting and measuring neuronal signals

The signals transmitted through a neuron are directly related to the $Na^+$ and $K^+$ ions, and the membrane potential they generate, as explained above. Detecting and measuring neuronal signals, therefore, means detecting and measuring the presence of these positively charged ions and the changes they undergo. A measuring device that responds to a specific species or situation, in this case the $Na^+$ and $K^+$ ions or the resulting membrane potential, is known as a sensor. A sensor consists meanly of two parts: a sensing element and a signal transducer. The sensing element responds to the species or situation being measured, known as the analyte. This response is converted by the signal transducer into an observable and measurable signal. The signal of many transducers is an electrical one, enabling easy integration in any electrical circuit to obtain direct electronic readout of the sensor.[11] In most sensors, however, the transducer is integrated with the sensing element, making it hard to recognize.
The detection characteristics of a sensor depend on many parameters and properties. The most important parameters are the sensitivity and the detection limit. The sensitivity, the change of sensor signal with respect to changing values of analyte, should be high enough to obtain accurate results. Closely related to the sensitivity is the detection limit, the lowest value of analyte detectable, which should be as low as possible.[11,12] Sensors designed for measuring and detecting neuronal signals also need to have a fast response and high time resolution. Since the change in membrane

potential during an action potential is only about 1 ms, a neuronal signal sensor should have a time resolution of around 0.1 ms.

### 2.2.1. Traditional methods

One of the traditional, electrophysiological, ways of detecting and measuring neuronal signals is by inserting a microelectrode into the neuron (see Figure 5: left). Such an intracellular microelectrode is typically a small glass capillary tube, filled with a conducting solution. It is pierced through the plasma membrane into the cytosol and measures the potential inside the neuron with respect to a reference electrode placed in the surrounding fluid. In this way, the membrane potential and action potential can be measured.[6,7] Unfortunately, neurons smaller than 10 µm in diameter are difficult to study with an intracellular microelectrode.[6]

Related to the microelectrode method is the patch-clamping technique (see Figure 5: left), which is used for studying ion channels in the plasma membrane. A similar glass microelectrode, but with a somewhat larger tip, is pressed against the plasma membrane, without piercing through it. In this way, it is possible to study the electrical behaviour of the small patch of membrane covered by the electrode, like the ion currents due to the ion flux across the membrane. Different configurations are possible, like detaching the patch of membrane from the cell, which makes the patch-clamping technique very versatile and applicable in many studies.[6]

Intracellular microelectrodes and the patch-clamping technique are in principle only

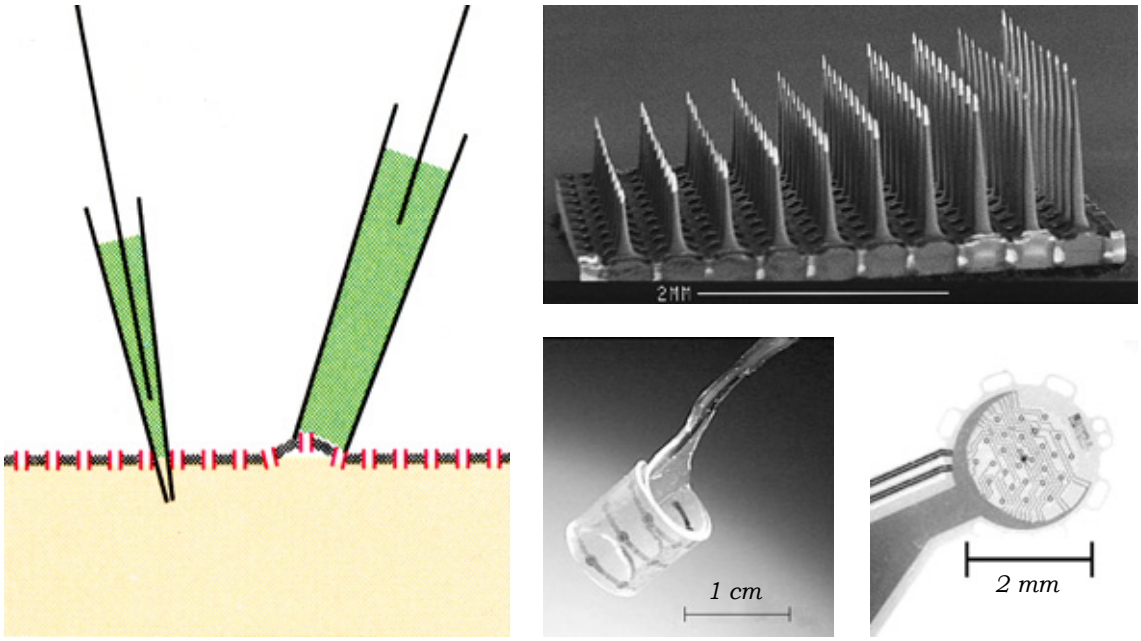


**Figure 5: Traditional neural interfaces.** *Left: Schematic illustration of an intracellular microelectrode (left) and the patch-clamp technique (right), after Darnell[7] Right: Scanning electron microscope picture of a Utah array[13] (top) and photos of a cuff electrode (bottom left) and a sieve electrode (bottom right).[15]*

suitable for the study of neurons *in vitro*. Therefore, they do not really have a future as the basis of implantable neural interfacing systems. Many sensors used nowadays for detecting and measuring neuronal signals, however, are related to microelectrodes. One of the basic sensors is based on microwire electrodes and is used for extracellular recording of the potential fields around neurons. Generally, a few thin wires (~40 µm) are bundled together, which enables recording of multiple neurons at the same time. Microwires are typically used to access deep brain structures. The precise location of the microwire electrode tips, however, is usually not known, since the wires can move apart from each other during and after implantation.[4] A more fixed structure can be obtained using technologies from silicon semiconductor industry. Arrays with many silicon microelectrodes, each of ~15 µm, have been fabricated with precisely defined distances between the electrodes. Commonly used arrays are the Michigan array (two-dimensional structure) and the Utah array (three-dimensional structure)[13] (see Figure 5: right - top). With these arrays, also a much higher density of electrodes can be obtained, resulting in a higher spatial resolution.[4,14]
Sensors based on microelectrodes are mainly used as brain implants. To study neurons in nerves, other types of sensors are used, usually based on cuff electrodes and sieve electrodes (see Figure 5: right - bottom). Cuff electrodes are electrodes placed inside a cylindrical tube that is wrapped around a nerve. In this way, the extracellular potentials around neurons in nerves can be measured.[4,5,14] Another way of measuring the extracellular potential around neurons is by use of sieve electrodes, metallised holes in a thin perforated planar sheet. When nerves of vertebrates are cut, the two ends are able to regenerate the nerve if they are in close proximity. Sieve electrodes placed between the ends of the nerve facilitate regeneration through the holes. Once the nerve is regenerated, it holds the sieve electrodes into place and creates an interface between the electrodes and the nerve.[4,14,15]

One of the most important issues for an implanted sensor is the biological response to it. Most microelectrode arrays perform well initially. Acute inflammations usually do not reduce performance. In the long term, however, chronic inflammations often result in generation of a compact fibrous sheath surrounding the implant. This encapsulating sheath insulates the electrodes from the neurons. As a result, the sensors performance severely decreases, leading to loss of signal and signal quality over time. In addition, chronically implanted microelectrode arrays may also lead to a significant reduction in the number of neurons in the vicinity of the implant.[4]
Biocompatible materials induce less inflammation at the implantation site. Therefore, studies have been carried out into microelectrode arrays coated with biocompatible materials. Most studies rely on biocompatible organic polymers,[4] like polyethylene glycol (PEG), poly(styrene sulphonate) (PSS), polyethyleneimine (PEI) with laminin, and even mixed self-assembled monolayers of thiolated poly(alkylthiophene) and functionalized alkanethiols[16]. The latter not only improves the biocompatibility of the electrodes, it also enhances the attachment of neurons to the electrode. A similar result has been obtained with electrodes coated with poly(3,4-ethylenedioxythiophene) (PEDOT) incorporating bioactive peptides.[17] Also coatings containing anti-inflammatory agents, using organic polymer matrices, have been studied.[4]

Inflammations are not only caused by materials that are not biocompatible. Also shear forces induced from relative motion of the implant contribute to inflammations. A disadvantage of silicon microelectrode arrays is their relative rigidity. The mechanical mismatch between these rigid electrodes and soft biological tissue is rather large. Silicon microelectrode arrays, therefore, aggravate inflammation at the implantation site. Flexible sensors can reduce this kind of inflammation.[4] Therefore, polyimide-based microelectrode arrays have been developed.[18] Also other materials have been studied, like polymer hydrogel electrodes of PEDOT:PSS and polypyrrole,[19] that might be suitable for usage in flexible microelectrode systems, therefore inducing less inflammations and scar formation.

All systems for measuring and detecting neuronal signals described so far are relatively large compared to the neurons they are measuring. As mentioned by Cheung[4] however, a theoretical analysis of the extracellular potentials around neurons has been shown that it is distorted by the presence of a large electrode. Potentials in front of the electrode are increased, whereas potentials behind the electrode are nearly completely shielded. To minimize this distortion and obtain more accurate measurement values, the electrode should be scaled to a width in the order of the neuron radius. In addition, a small implant displaces and damages much less surrounding tissue than a larger one does, reducing the amount of inflammations.[4] Moreover, with small electrodes it will be really possible to measure on single neurons, instead of a large bundle of neurons, and, therefore, to obtain a much higher resolution. Unfortunately, it is not easy to scale down the described systems to the desired level.
Another, even more important, issue is the magnitude of the neuronal signals. The membrane potential and action potential are only in the order of tens of millivolts. All systems described so far are based on rather large electrodes. These electrodes measure the neuronal signals directly, without any kind of amplification. The magnitude of the neuronal signals is, however, relatively low. Therefore, noise might play a significant role in the output signal of the sensor, especially when measuring on a single neuron. To prevent this, the neuronal signal should be converted into an amplified electrical signal. In this way, an accurate and measurable output signal can be obtained from the sensor.

### 2.2.2. Field-effect transistor

Amplification of the neuronal signals into measurable electrical signals can be achieved by using a field-effect transistor setup. One of the main advantages of a field-effect transistor setup is that a field-effect transistor is easily scaled down to a level desired for neural interfacing.
In a field-effect transistor, a semiconductor is separated from an electrode, the gate, by an insulating layer (see Figure 7: left - top). The semiconductor is also in direct contact with two other electrodes, the source electrode and the drain electrode. When a voltage is applied to the drain electrode, generating an electric field between the source and drain, charge carriers move through the semiconductor towards the electrodes, resulting in a source-drain current ($I_{SD}$). The source-drain current consists

of a bulk current and a field-effect current. The bulk current is a current through the entire thickness of the semiconductor, which depends on the number of free charge carriers in the material. The field-effect current is a current through the semiconductor near the interface with the insulator.[20,21]
The field-effect current can be influenced by the gate electrode. A voltage on the gate electrode results in a second electric field perpendicular to the source-drain current. Depending on the sign of the applied voltage, charge carriers will either be accumulated at or depleted from the semiconductor-insulator interface. This can be understood from the energy band diagram of the gate-metal, insulator and semiconductor (see Figure 6). When the Fermi energy levels ($E_F$) of the semiconductor and the metal are equal, the energy bands of the semiconductor are flat, also at the semiconductor-insulator interface (flat-band condition). When a negative voltage is applied to the metal, the energy bands in the semiconductor bend upwards at the semiconductor-insulator interface in an attempt to again align the Fermi energy level with that of the metal. Hence, additional positive charge carriers, supplied by the source- and drain electrodes, are accumulated at the semiconductor-insulator interface. On the other hand, when a positive voltage is applied to the metal, the energy bands in the semiconductor bend downwards and the positive charge carriers are depleted from the semiconductor-insulator interface. Most semiconductors initially do not have their Fermi energy level equal to that of the metal and are already in accumulation or depletion when no voltage is applied to the metal. To obtain flat-band condition in these semiconductors, a voltage equal to the difference in the Fermi energy levels (the flat-band voltage: $V_{FB}$) has to be applied to the metal.[21]
When the charge carriers are accumulated at the interface between the semiconductor and the insulator, they form a conduction channel that gives rise to the field-effect current. Since the field-effect current is much higher than the bulk current, the source-drain current is highly increased. Depletion of the charge carriers, on the other hand, results in a decreased source-drain current equal to only the bulk current.

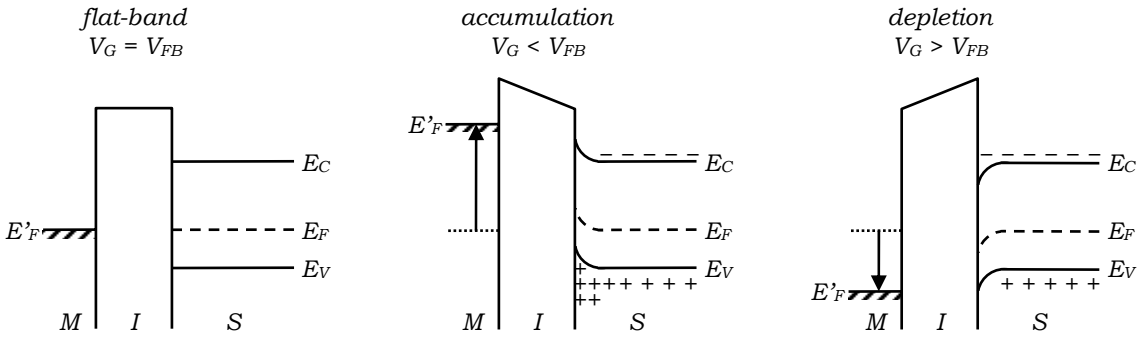


**Figure 6: Energy band diagram of a field-effect transistor.** *Energy band diagrams of the metal (M), insulator (I) and semiconductor (S) in the flat-band condition ($V_G = V_{FB}$) (left) and when the semiconductor is in accumulation ($V_G < V_{FB}$) (middle) and in depletion ($V_G > V_{FB}$) (right). $E'_F$ depicts the Fermi energy level of the metal and $E_F$ that of the semiconductor. $E_C$ and $E_V$ are the energy levels of the conduction band and the valence band of the semiconductor respectively.*

When a large enough positive voltage is applied to the gate electrode, the entire thickness of the semiconductor will be depleted from mobile charge carriers and the source-drain current becomes zero.[20,21]
When characterizing a field-effect transistor, several parameters are of importance. Most important is the threshold voltage ($V_{TH}$), sometimes called the switch-on voltage. The threshold voltage is the voltage at which accumulation starts to occur at the semiconductor-insulator surface, that is, there is no energy band bending in the semiconductor. Below $V_{TH}$ the variation of the field-effect current with the gate voltage is zero, while the field-effect current increases with the applied gate voltage above $V_{TH}$. Another important parameter is the switch-on voltage ($V_{SO}$), sometimes called the pinch-off voltage. The switch-on voltage is the voltage at which the entire thickness of the semiconductor is depleted from charge carriers and the source-drain current becomes zero.[20] Below $V_{SO}$ the transistor is said to be in its OFF-state and above $V_{TH}$ in its ON-state. An important parameter related to this is the ON-OFF ratio, the ratio between the source-drain current in the ON-state and the OFF-state.
A field-effect transistor can operate in the linear or in the saturation regime. In the linear regime the source-drain voltage ($V_D$) is (much) smaller than the applied gate voltage ($V_G$): $|V_D| < |V_G|$. In the saturation regime, on the other hand, $|V_D| > |V_G|$. A field-effect transistor can be considered as a parallel-plate capacitor, where the gate is one plate and the conduction channel in the semiconductor is the other plate. Therefore, in the linear regime, the source-drain current is given by

$$I_{SD} = \frac{W}{L} \mu C_I (V_G - V_{TH}) V_D \qquad (3)$$

and in the saturation regime by

$$I_{SD} = \frac{W}{2L} \mu C_I (V_G - V_{TH})^2 \qquad (4)$$

where $W$ is the channel width, $L$ is the channel length, $\mu$ is the field-effect mobility of the charge carriers and $C_I$ is the insulator capacitance per unit area.

### 2.2.3. Field-effect transistors as sensor

A transistor clearly shows amplification behaviour, since a small gate voltage can be used to control a large source-drain current, by controlling the conduction channel.[21] In a similar way, the $Na^+$ and $K^+$ ions involved in the membrane potential and action potential can control the conduction channel. In general, any charge creates an electric field in the space surrounding it. When the gate electrode of a field-effect transistor is replaced by the plasma membrane of a neuron, the charges at the outside of the membrane create an electric field similar to that of the gate electrode itself. This field again influences the conduction channel at the semiconductor-insulator interface, which is called capacitive coupling (see Figure 7: left - bottom). When the neuron is at rest, the outside of its plasma membrane is positively charged (see again Figure 3). These charges will induce depletion of charge carries at the semiconductor-insulator interface. When the neuron fires, an action potential is generated. Depolarization now results in negative charges at the outside of the plasma membrane. These negative charges will induce accumulation, leading to formation of the conduction channel and an increase in source-drain current. Hyperpolarization

and return to the resting potential induce depletion again, resulting in decrease of the source-drain current to its original value. The source-drain current, therefore, reflects the changes in the membrane potential and follows the shape of the action potential (see Figure 7: right).
Generation of an action potential involves little amount of charges. Only about 6000 $Na^+$ ions pass the membrane per ion channel after opening of such a channel.[7] Due to

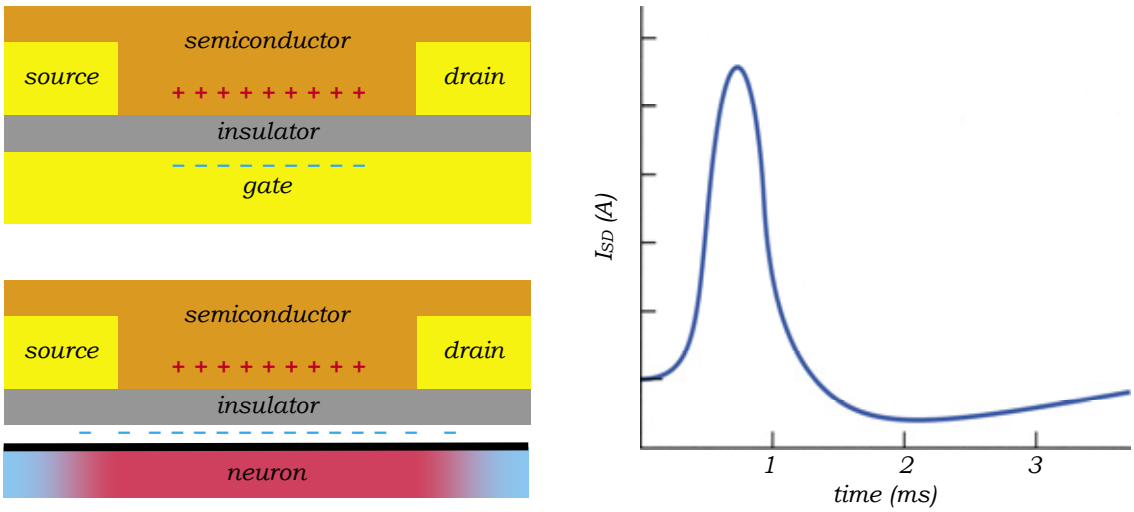


**Figure 7: Field-effect transistor.** *Accumulation of charge carriers at the interface of semiconductor and insulator, resulting in the formation of a conduction channel, due to a negative voltage on the gate electrode (left: top). The same situation is obtained when the gate is replaced by a neuron with a depolarized plasma membrane (left: bottom). Here the semiconductor is a p-type doped semiconductor with positive charge carriers. The source-drain current ($I_{SD}$) reflects the changes in the membrane potential and follows the shape of the action potential (right) (compare Figure 3).*

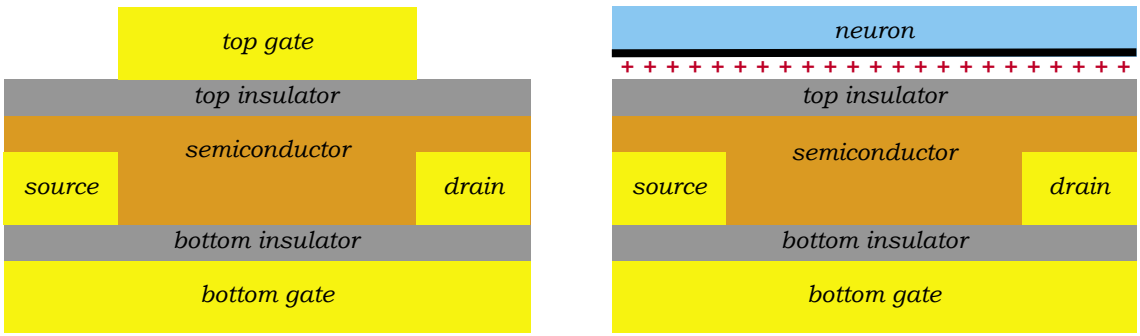


**Figure 8: Dual-gate field-effect transistor.** *A dual-gate field-effect transistor has a bottom contact geometry together with an extra insulating layer and gate on top of the semiconductor (left). In a sensor for detecting and measuring neuronal signals, the top gate is replaced by a (resting) neuron (right). The bottom gate controls the threshold voltage.*

the amplification behaviour of the field-effect transistor, this is, however, sufficient to obtain a measurable change in source-drain current.
To obtain a sensor with an even higher sensitivity, a dual-gate field-effect transistor can be used. A dual-gate field-effect transistor has a bottom contact geometry together with an extra insulating layer and gate on top of the semiconductor (see Figure 8). The main advantage of a dual-gate field-effect transistor is the possibility to use the second gate to accurately control the threshold voltage.[22-26] Around the threshold voltage the sensitivity of the sensor is very high, since the presence of a small amount of analyte is enough to induce a large increase in current (see Figure 9: left). By changing the threshold voltage, the high sensitivity can be shifted to a concentration region of interest (see Figure 9: right), for example a very low concentration to obtain a low detection limit. However, the sensitivity in other regions can also be increased by changing the threshold voltage again, leading to a large range with highly improved sensitivity.

### 2.2.4. Transistor-based neuronal sensors

The semiconductor in a (dual-gate) field-effect transistor can in principle be made out of any semiconducting material. Traditionally in semiconductor industry, silicon is the material of choice. Many different silicon field-effect transistors have already been reported for detecting and measuring neuronal signals, yet none of them clearly make

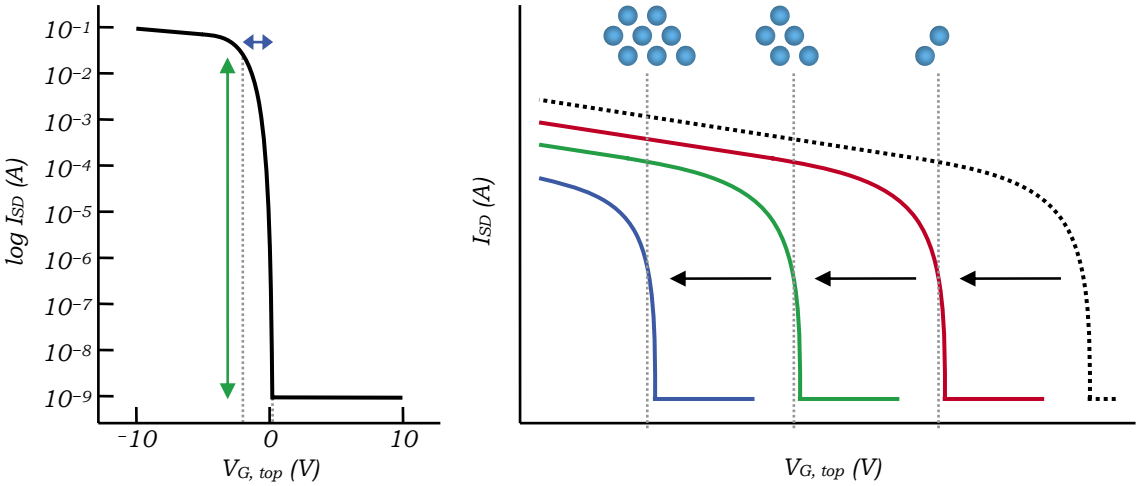


**Figure 9: High sensitivity and threshold voltage shift.** *The sensitivity of a sensor is highest around the threshold voltage, where the variation of the source-drain current ($I_{SD}$) is large. This can be seen from the transfer characteristics of a field-effect transistor (left). A small (additional) voltage on the top gate of ~1 Volt, corresponding to the presence of a small amount of analyte, (blue arrow) results in a large change in source-drain current of many orders of magnitude (green arrow). The threshold voltage can be shifted by applying a voltage on the bottom gate (right). The black, dotted curve shows a typical source-drain current without an active bottom gate. Only the top gate, or the presence of analyte molecules, induces changes in source-drain current. By applying a voltage on the bottom gate, the threshold voltage, and therefore the region of high sensitivity, can be shifted to an analyte concentration of interest (red, green and blue curves).*

use of the dual-gate effect. Nevertheless, a network of cultured pond snail neurons has been studied successfully with one of these sensors.[27] In another study, a multi-transistor array has been used to obtain a two-dimensional mapping of neuronal activity of single pond snail neurons and a small network of neurons.[28] Also work on cultured mammalian neurons has been reported based on an array of field-effect transistors.[29] Single mammalian neurons have also been studied with an array of electrolyte-oxide-silicon field-effect transistors.[30] In a more recent study, based on silicon nanowire field-effect transistors, neuronal signals have been detected and measured from the axon and dendrites of single mammalian neurons.[31]

Nowadays, organic materials, like polymers, have gained more and more attention as the semiconducting material in (dual-gate) field-effect transistors. These kinds of materials can be easily deposited on a variety of substrates, including flexible ones, using low temperature processes.[32] As a result, low cost fabrication techniques can be used for producing flexible sensors based on these materials. Moreover, a wide choice of molecular structure, including the possibility to build in side chains and end groups, enables films to be produced with (grains of) specific physical and chemical properties.[33] In addition, large area coverage and controlled layer thicknesses can simply be achieved.

Not all organic materials are semiconducting. Some show insulating properties and can be easily used as the insulator in a field-effect transistor, owing to their straightforward solution processability. Another advantage of these organic materials is the easy adaptation of the thickness of the insulating layer via spincoating. This is important for the quantitative influence the analytes will have on the conduction channel in the semiconductor.

The top insulating layer in a dual-gate field-effect transistor not only acts as an insulator, but also as a protection layer for the semiconductor. Next to this, it functions as the attachment site for the plasma membrane of the neurons. The use of organic materials as the insulating layer is an advantage for attachment, since these materials are easily functionalized. Therefore, the right material can be chosen for neuronal growth, obtaining intimate contact between the neuron and the sensor. Moreover, in contrast to many inorganic materials, organic (semiconducting) polymers are biocompatible. For example, studies on polyimide[34] and SU-8[35] show almost no cytotoxicity responses to these materials and many synthetic polymers are available for biocompatible drug carriers[36]. Together with their flexibility, organic polymers will therefore induce less inflammations and scar formation. Inflammations might even be reduced actively by proper functionalization of the polymers or by inclusion of anti-inflammatory agents.

Organic field-effect transistors for measuring and detecting neuronal signals have not been reported yet. A pentacene organic field-effect transistor, however, has been developed, encapsulated with parylene.[37] According to the authors, results are promising for use of this field-effect transistor in flexible biomedical microimplants and neural prostheses, but measurements on neurons have not been carried out. In a more recent study a similar pentacene field-effect transistor has been used for the stimulation of neurons.[38] This field-effect transistor, however, is not directly in

contact with the neuron, but connected to a cuff electrode. It is only used to obtain an adjustable current that is directed to the cuff electrode in order to induce action potentials in the neurons. Furthermore, the authors excite a complete nerve, instead of individual neurons.

## 2.3. Outline of the work

The work described here is a first step towards a new type of sensor to detect and measure neuronal signals, based on polymeric dual-gate field-effect transistors. First of all, the semiconducting and insulating organic polymers have been studied, in a few differently composed transistors, for their dual-gate field-effect transistor characteristics. Essential for neurons to survive on top of the field-effect transistor is an aqueous environment with certain ingredients, especially sodium- and potassium salts. To avoid problems in this aqueous environment, water needs to be blocked from both the gate electrode and the source- and drain electrodes of the field-effect transistor. A major part of this work, therefore, has been devoted to the selection of a suitable water blocking top insulator layer. The influence of the salts on the transistor characteristics has also been studied. In order to study these influences systematically, a flow channel setup has been developed to supply solutions to the transistor in a standard, defined way.

# 3. Experimental

Three different combinations of semiconducting and insulating organic polymers have been studied for their dual-gate field-effect transistor characteristics. The water blocking capability of the semiconductor and the insulator has also been studied extensively. Eventually, the influence of water and some salt solutions on the field-effect transistor characteristics has been studied. In the following, a detailed description of the manufacturing of the transistors and the materials used is presented. Also, the characterization of the transistors is shortly described, including a description of the manufacturing of the flow channels for the flow channel setup.

## 3.1. Dual-gate field-effect transistors

Dual-gate field-effect transistors were manufactured from semiconducting and insulating organic polymers. The semiconducting polymers used were poly[2-methoxy-5-(2'-ethylhexyloxy)-1,4-phenylene vinylene] (MEH-PPV) and poly[*N*,*N*'-bis(4-butylphenyl)-*N*,*N*'-bis(phenyl)benzidine] (PAA). MEH-PPV had been synthesized in the Polymer Chemistry department at the University of Groningen. PAA had been purchased from American Dye Source, Inc. as Hole Transport Polymer ADS254BE with a molecular weight of 10,000 – 70,000. The insulating polymers used were poly(methyl methacrylate) (PMMA) and the copolymer poly(vinylidene difluoride–trifluoroethylene) (P(VDF-TrFE)). PMMA had been purchased from Aldrich with an average molecular weight of 120,000. The random copolymer P(VDF-TrFE) had been purchased from Solvay Duphar, Belgium with a 50%–50% ratio of VDF and TrFE. See Figure 10 for the structures of MEH-PPV, PAA, PMMA and P(VDF-TrFE).

The dual-gate field-effect transistors were manufactured on heavily doped n-type prime silicon wafers with thermally grown silicon oxide on top, purchased from Silicon Quest International. Silicon oxide layers were either 300 nm, 500 nm or 1000 nm thick. The silicon wafers acted both as the substrate and as the bottom gate (silicon) with bottom insulator (silicon oxide).

All wafers were cleaned following a typical cleaning procedure. First, the wafers were rinsed with acetone and 2-propanol. Next, the wafers were submerged in a 65 °C basic piranha solution, composed of 7 parts demineralized (demi) water, 1 part 30% hydrogen peroxide and 1 part 25% ammonia, for typically 1 – 2 minutes. After a 10 seconds dip in demi water, to quench the basic piranha, the wafers were rinsed with 2-propanol again. Subsequently, the wafers were wetted with a few drops of 1,1,1,3,3,3-hexamethyldisilazane (HMDS) (purchased from Merck KGaA) and dried at a 100 °C hotplate in order to hydrophobize the surface with methyl groups. Any remaining HMDS was washed away by rinsing the wafers with 2-propanol.

A solution of 7 parts negative tone photoresist (ma-N 1410, Micro Resist Technology GmbH) and 1 part thinner for photoresist (ma-T 1046, Micro Resist Technology GmbH) was prepared and thoroughly mixed on a roller mixer. The photoresist solution was

spincoated in air on the cleaned wafers. Next, the wafers were soft baked at a 100 °C hotplate for 90 seconds, followed by cooling down in air. The wafers with photoresist on top were exposed to broadband UV radiation (192 mJ $cm^{-2}$ at 405 nm) through a clear field mask using a Süss MicroTec photolithography apparatus. Immediately after exposure the wafers were developed by submersion in photoresist developer (ma-D 533S, Micro Resist Technology GmbH) for 45 seconds, followed by rinsing with demi water.
Dry developed wafers were placed in a homebuilt metal evaporation system. A thin layer of ~1 nm chromium (Cr) was evaporated at the wafers, followed by ~50 nm of gold (Au) at a pressure of typically $1\times10^{-6}$ mbar. Next, the wafers were placed in an ultrasonic bath of acetone for 20 minutes to lift-off the photoresist, followed by a short rinse with acetone. Subsequently, the wafers were cut in 3 × 3 cm square samples according to the bottom contact pattern. The samples were rinsed with acetone to remove particles from the surface that were created by the cutting procedure.
Before spincoating the polymers on the samples, the samples were thoroughly cleaned. First, the samples were successively placed in an ultrasonic bath of acetone for 5 minutes, submerged in demi water for 8 minutes and placed in an ultrasonic bath of 2-propanol for 5 minutes. Next, the samples were exposed to UV-ozone for 20 minutes. Subsequently, the samples were submerged in 65 °C basic piranha for 45 seconds, followed by a 10 seconds dip in demi water and rinsing with 2-propanol. Afterwards, the wafers were wetted with HMDS, dried at a 100 °C hotplate and rinsed with 2-propanol.
Solutions of MEH-PPV dissolved in toluene, PMMA dissolved in methyl ethyl ketone (MEK), P(VDF-TrFE) dissolved in MEK, and PAA dissolved in chloroform were filtered with PTFE filters. Typically, 0.45 µm, 1 µm or 5 µm filters were used. Subsequently, the semiconducting polymer (MEH-PPV or PAA) was spincoated on the cleaned samples in a nitrogen atmosphere. The insulating polymer (PMMA or P(VDF-TrFE)) was spincoated subsequently on top of the semiconductor.
Top gate electrodes were evaporated on the samples in the homebuilt metal evaporation system. A layer of ~80 nm silver (Ag) was evaporated at a pressure of typically $1\times10^{-6}$ mbar.
Layer thicknesses of the spincoated polymers were determined on glass in air at room temperature with a Dektak 6M Stylus Profiler. Transfer- and output characteristics were measured in vacuum ($<2\times10^{-6}$ mbar) in a homebuilt four-probe measurement system using a Keithley 4200 Semiconductor Characterization System.

## 3.2. Water blocking layers

All experiments related to the water blocking capability of the insulating layer were carried out on standard field-effect transistor substrates, provided by Philips Research Laboratories Eindhoven as part of a 6-inch wafer. These 13 × 17 mm substrates consisted of heavily doped n-type silicon with thermally grown silicon oxide (200 nm or 2 µm) on top. A gold interdigitated finger pattern had been prefabricated on top of the silicon oxide with a constant channel width of 10 mm and a varying channel

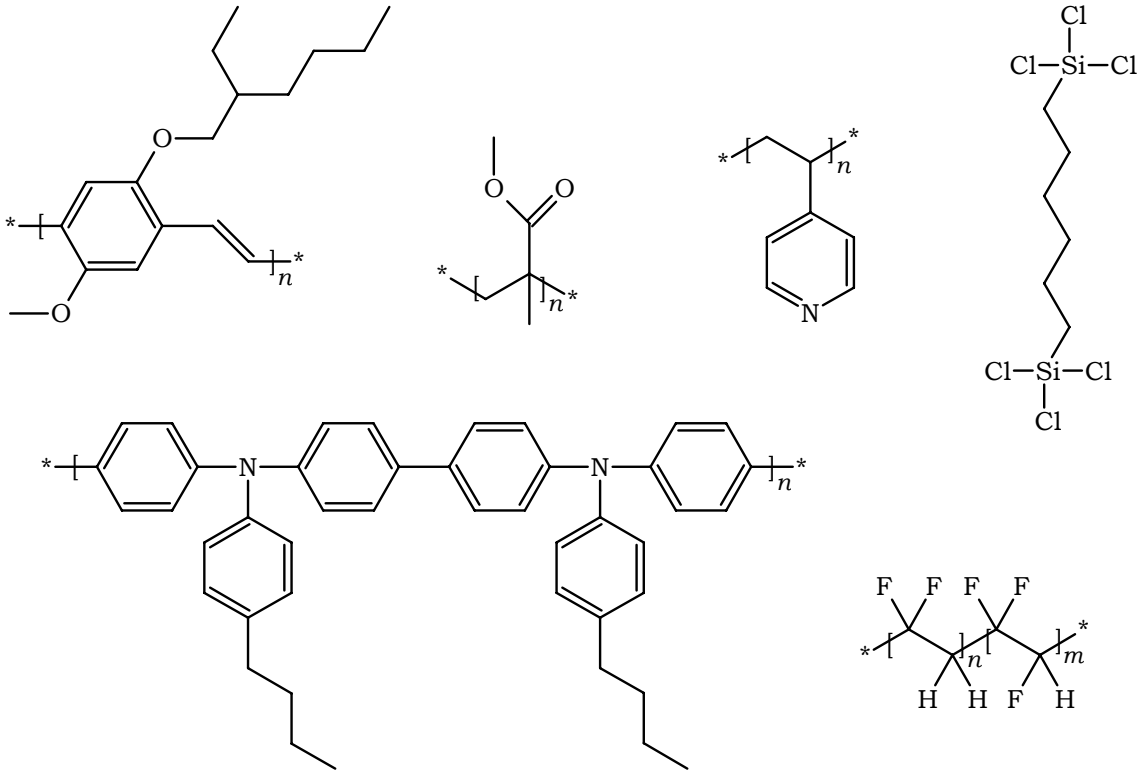


**Figure 10: Chemical structures.** *The chemical structures of MEH-PPV (top: left), PMMA (top: middle left), P4VP (top: middle right), crosslinker (top: right), PAA (bottom: left) and P(VDF-TrFE) (bottom: right).*

length of 5 – 40 µm (200 nm silicon oxide substrates) or a constant channel length of 10 µm (2 µm silicon oxide substrates).

The substrates were cleaned following a standard cleaning procedure. First, the substrates were successively placed in an ultrasonic bath of acetone for 5 minutes, submerged in demi water for 8 minutes and placed in an ultrasonic bath of 2-propanol for 5 minutes. Next, the substrates were exposed to UV-ozone for 20 minutes to pre-clean them. Subsequently, the substrates were submerged in 65 °C basic piranha for typically 60 seconds to thoroughly remove any remaining organics. After a 15 seconds dip in demi water, to quench the basic piranha, the substrates were rinsed with 2-propanol. Then, the substrates were exposed to UV-ozone for another 20 minutes to hydrophilize the surface. Afterwards, the substrates were wetted with HMDS and dried at a 100 °C hotplate in order to hydrophobize the surface again. Any remaining HMDS was washed away by rinsing the substrates with 2-propanol.

For some tests and experiments, thorough cleaning was less important. Therefore, the basic piranha and second UV-ozone treatments were omitted in some cases. When substrates were recycled, they were first cleaned in an ultrasonic bath of a suitable solvent, like chloroform or chlorobenzene, to remove all polymer layers. Sometimes (gentle) wiping with a solvent-soaked cotton swab was necessary to remove all

polymer. Substrates free of polymer were further cleaned by following the standard cleaning procedure again.
The water blocking capability of several materials was studied. The materials used were PMMA (as described above), PMMA e-beam photoresist and poly(4-vinylpyridine) (P4VP). PMMA e-beam photoresist had been purchased from Allresist GmbH as AR-P 679.02, a solution of PMMA (molecular weight: 950,000) dissolved in ethylacetate and *n*-butylacetate. P4VP had been purchased from Sigma-Aldrich with a typical molecular weight of 160,000. In some experiments, the insulators were combined with the crosslinker 1,6-bis(trichlorosilyl)hexane, purchased from Aldrich at 97% purity. See Figure 10 for the structures of P4VP and the crosslinker.
In most experiments, the insulating polymers were spincoated directly on top of the cleaned substrates in a nitrogen atmosphere. In some experiments, a single-gate field-effect transistor was manufactured by first spincoating PAA followed by spincoating an insulating polymer on top, again in a nitrogen atmosphere. As before, solutions were filtered with PTFE filters prior to spincoating. PMMA was dissolved in MEK or *n*-butyl acetate, PAA in chloroform and P4VP in ethanol. PMMA e-beam photoresist was purchased in solution. The crosslinker was typically added to the insulating polymer solutions (0.35 µl crosslinker per 1 mg polymer) directly before filtering in order to avoid early crosslinking in solution. When the crosslinker was spincoated as a separate layer, the crosslinker was diluted with MEK. Samples including layers with crosslinker were annealed after spincoating at a 100 °C hotplate for typically 10 minutes, either in air or in a nitrogen atmosphere.
Layer thicknesses of the spincoated polymers were determined on glass in air at room temperature with a Dektak 6M Stylus Profiler. Transistor measurements to study the water blocking capability of the layers were carried out at room temperature in the homebuilt measurement system using a Keithley 4200 Semiconductor Characterization System.

## 3.3. Salt solutions

All experiments related to the influence of water and salt solutions were carried out on cleaned standard field-effect transistor substrates, as described above. Single-gate field-effect transistors were manufactured from PAA and PMMA, as explained above. Layer thicknesses of the spincoated polymers were determined on glass in air at room temperature with a Dektak 6M Stylus Profiler.
The influence of demi water, sodium chloride (NaCl) solutions and potassium chloride (KCl) solutions on the single-gate field-effect transistors was studied. NaCl and KCl had been purchased from Merck KGaA. The salts were dissolved in demi water to obtain solutions of 1, 10, 100 and 1000 mM (NaCl), and solutions of 0.78, 7.8, 78 and 780 mM (KCl). The transfer- and output characteristics of the single-gate field-effect transistors were studied in air at room temperature in the homebuilt measurement system using a Keithley 4200 Semiconductor Characterization System.
The solutions were applied to the transistor surface drop by drop with a glass pipette and removed with either the glass pipette or a tissue. Later, a flow channel setup (see

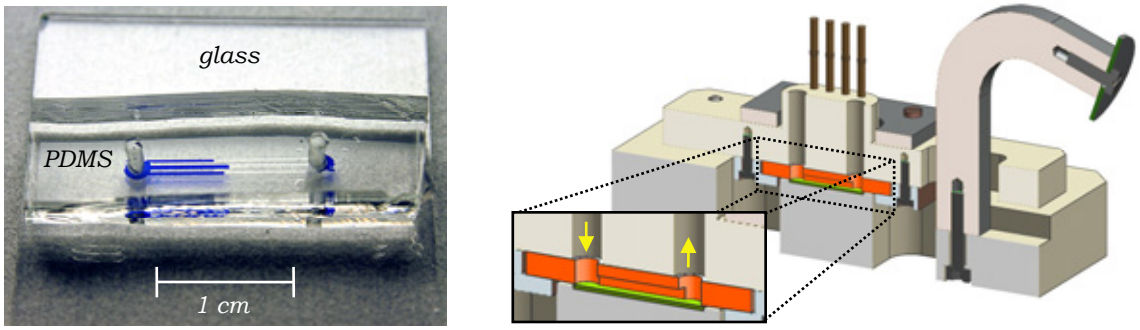


**Figure 11: Flow channel setup.** *Illustration of the cross-section of the flow channel setup (right), showing a PDMS block (orange) on top of the transistor device (green) (see also inset). The PDMS block contains a small channel connecting two reservoirs. The reservoirs are accessed through the two holes in the PDMS block and the flow channel setup. Fluids can be applied to the transistor surface through the channel in the PDMS block, as shown by the photo of a PDMS block on glass with the channel between the reservoirs half filled with ink (left). The four brown 'pipes' in the illustration are the probes for contacting the source- or drain electrodes on the sample.*

Figure 11) was used to supply the solutions to the transistor in a standard, defined way in order to study the influence of the solutions more systematically.

## 3.4. Solution supplying channel

The flow channel setup contains a small channel to supply fluids to the transistor surface (see Figure 11). This channel was made out of a small piece of poly(dimethylsiloxane) (PDMS). A standard method was used to manufacture these channels for the flow channel setup.

PDMS channels were made from a mould that was manufactured on top of a silicon wafer. The test grade silicon wafer had been purchased from Silicon Quest International and was thoroughly cleaned. First, a wafer was rinsed with acetone and 2-propanol. Next, the wafer was submerged in 65 °C basic piranha for 3 minutes, followed by a 15 seconds dip in demi water and rinsing with 2-propanol. Afterwards, the wafer was wetted with HMDS, dried in air at room temperature and rinsed again with 2-propanol.

The negative photoresist SU-8 (SU-8 2025, MicroChem), was spincoated on the cleaned wafer and soft baked at a 95 °C hotplate for 8 minutes. The wafer with photoresist on top was exposed to broadband UV radiation (240 mJ $cm^{-2}$ at 405 nm), through a homebuilt dark field mask with the proper channel configuration, using a Süss MicroTec photolithography apparatus. Immediately after exposure the wafer was baked at a 95 °C hotplate for 5 minutes to initiate the thermally driven crosslinking catalyzed by the strong acid formed during exposure. Next, the wafer was developed by submersion in photoresist developer (mr-Dev 600, Micro Resist Technology GmbH) for 4 minutes, followed by a rinse with developer and 2-propanol. Finally, the wafer was hard baked at a 150 °C hotplate for 5 minutes.

The developed wafer was exposed to UV-ozone for 10 minutes to hydrophilize the SU-8 surface. Next, the wafer was placed in a petridish on a 120 °C hotplate for 40 minutes in a nitrogen atmosphere. The wafer was surrounded by a few drops of trichloro(1*H*,1*H*,2*H*,2*H*-perfluorooctyl)silane (purchased from Aldrich), which would attach to the SU-8 facilitating the peal-off of the PDMS from the SU-8 mould later on.
Pure PDMS, purchased from Dow Corning as Sylgard 184 Base Silicone Elastomere, was mixed with curing agent (Sylgard 184 curing agent Silicon Elastomere, Dow Corning) in a 10:1 ratio and left in a vacuum excicator for several hours to remove air bubbles. Eventually, the PDMS was poured onto the wafer in a plastic petridish. The PDMS was left for curing in a 60 °C oven for 10 hours. Finally, the solidified PDMS was removed from the SU-8 mould and cut into rectangular blocks that fitted in the flow channel setup. In the end, small 1.3 millimetre diameter holes were drilled into the PDMS blocks to be able to supply fluids to the reservoirs and the channel. Before using the PDMS blocks, the reservoirs and channel were hydrophilized by exposure to UV-ozone for typically 5 – 10 minutes.

# 4. Results and discussion

This chapter presents the main results from the experiments carried out. First, the dual-gate field-effect transistor characteristics of three different combinations of semiconducting and insulating organic polymers are presented. Then, the behaviour of water exposed to the currents and voltages present in the field-effect transistors are highlighted. Next, the experiments that have been done to obtain a water blocking insulator layer are described. Different insulator materials and combinations of these materials with a crosslinker have been tested. In the last section, the study on the influence of water and some salt solutions on the field-effect transistor characteristics is described.

## 4.1. Dual-gate field-effect transistors

Dual-gate field-effect transistors have been manufactured as described in the previous chapter. Transistors have been made of MEH-PPV/PMMA, MEH-PPV/P(VDF-TrFE) and PAA/PMMA.

### 4.1.1. MEH-PPV/PMMA

The transistors of MEH-PPV/PMMA have been manufactured on a wafer with 300 nm silicon oxide. The thickness of the spincoated layers was 86 nm for MEH-PPV and 354 nm for PMMA. The obtained transistors showed typical transistor behaviour for both the bottom channel and the top channel, as can be seen from the transfer- and output characteristics (see Figure 12).

Sweeping the bottom gate voltage ($V_{G,\,bottom}$), leaving the top gate floating, resulted in an ON-switch around $V_{G,\,bottom} = -5$ V. The source-drain current ($I_{SD}$) increased from $1\times10^{-9}$ A to about $1\times10^{-5}$ A, with a drain voltage ($V_D$) of −20 V, resulting in an ON-OFF ratio of $1\times10^{4}$. ON-currents were typically an order of magnitude lower when a $V_D$ of −2 V was applied. Current leakage to the bottom gate electrode remained below $1\times10^{-7}$ A. Low current leakages were confirmed by the output characteristics, since $I_{SD}$ started nicely from $V_D = 0$ V and showed reasonable linearity at low $V_D$ and saturation at high $V_D$.

Sweeping the top gate voltage ($V_{G,\,top}$), leaving the bottom gate floating, resulted in similar ON-switching. Since the bottom- and top insulator were of different material and thickness, the observed ON-switching could not directly be compared with the characteristics obtained for sweeping $V_{G,\,bottom}$. Therefore, the characteristics were corrected for the difference in capacitance between the bottom isolator and top isolator. It was assumed that the applied gate voltages induced charges in the semiconductor layer like it occurs in a parallel-plate capacitor, with a linear dependence between the (gate) voltage and the induced charges. Therefore, to compare the characteristics of the bottom- and top gate sweep, all applied $V_{G,\,top}$ have been multiplied by the ratio between $C_{bottom}$ and $C_{top}$.

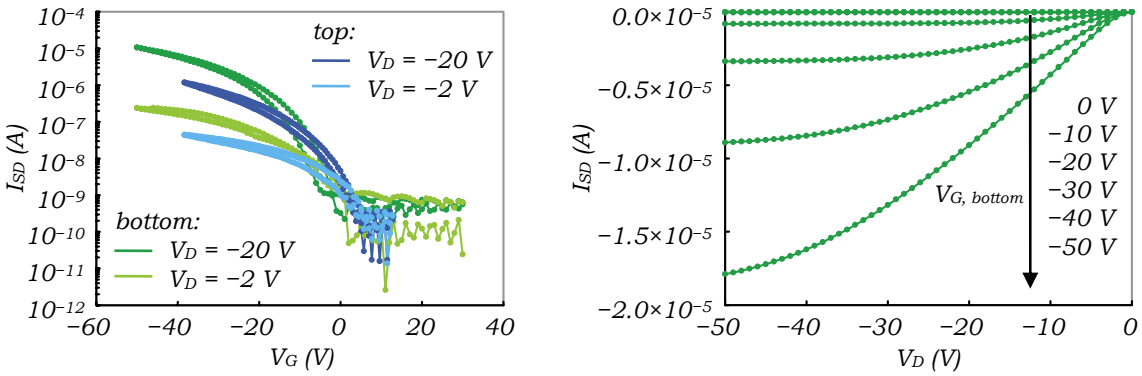


**Figure 12: Single channel characteristics of a dual-gate field-effect transistor.** *Transfer curves (left) and output curves (right) of an MEH-PPV/PMMA dual-gate field-effect transistor (L = 5 µm, W = 20 mm). The transfer curves plotted are of both the bottom channel (green) and top channel (blue) for $V_D$ = −2 V (light) and −20 V (dark). $V_{G,\ top}$ has been corrected for the difference in capacitance between the bottom- and top isolator. The output curves are from the bottom channel, for $V_{G,\ bottom}$ = 0 V, −10 V, −20 V, −30 V, −40 V and −50 V, but were similar for the top channel. In both graphs, $I_{SD}$ has been measured as the current going through the drain electrode. All measurements have been performed in vacuum (<2×10⁻⁶ mbar). The dual-gate field-effect transistors have been manufactured at a 300 nm oxide silicon wafer, with Ag top gate electrode. The thickness of the spincoated layers was 86 nm MEH-PPV and 354 nm PMMA.*

From the corrected characteristics it was observed that the ON-switching had been shifted to more positive $V_{G,\ top}$. OFF-currents were equal to the ones of the bottom gate voltage sweep, but ON-currents were about a factor of 5 – 10 lower. It is thought that this difference was mainly due to the difference in interface morphology. The top channel is always generated near the interface with the top insulating polymer, which has a rougher morphology than the silicon oxide. Therefore, the channel formation might not be optimal, resulting in a lower ON-current. Also the distance of the top channel to the source- and drain electrodes, which is likely to be larger than that of the bottom channel to the electrodes, could have played a role in the obtained lower ON-current for the top channel. Current leakage to the top gate electrode remained below $1\times10^{-8}$ A. This current leakage was a factor 10 lower than the leakage to the bottom gate electrode and could probably be linked to the lower capacitance of the top insulator.

The exact ON-currents for both channels depended on the channel width (*W*) and the channel length (*L*), as confined by the source- and drain electrodes. The shorter the channel, the higher the ON-currents, since less semiconductor material took part in conduction, as if the number of resistors in series was lower. On the other hand, the wider the channel, the higher the ON-currents, since more material took part in conduction, increasing the number of available (parallel) paths for conduction.

A few control transistors without the top gate electrode have been manufactured at the same wafer. These transistors are basically single-gate field-effect transistors coated with a layer of PMMA. These coated single-gate transistors showed very similar transistor characteristics as the dual-gate field-effect transistors, which had the top

gate electrode present. Therefore, it was concluded that evaporation of a silver (Ag) top electrode does not influence the transistor characteristics.

Transfer characteristics have also been determined with both gate electrodes connected. Sweeping $V_{G,\,bottom}$, with $V_{G,\,top}$ fixed at different voltages, resulted in transfer curves with ON-switching occurring at different $V_{G,\,bottom}$. Typically, ON-switching shifted from positive to negative $V_{G,\,bottom}$ when $V_{G,\,top}$ was increased from negative to positive values (see Figure 13: left). Such a result was also expected from theory, since both gates influence the charges in the semiconductor layer.

The voltage at which accumulation starts to occur, leading to a high increase in $I_{SD}$, is defined as the threshold voltage ($V_{TH}$). The threshold voltage can be extracted from the transfer curve of a transistor in accumulation. When the transistor operates in the saturation regime ($|V_D| > |V_G|$), the source-drain current depends quadratically on the gate voltage as $I_{SD} \sim (V_G - V_{TH})^2$ (see also again Equation 4). Plotting the square root of $I_{SD}$ against $V_G$ results in a straight line in the saturation regime. The intercept with the $V_G$-axis of the linear fit of this line is the threshold voltage of interest.[26] In this way, $V_{TH}$ at the different $V_{G,\,top}$ have been determined for several transistors and these $V_{TH}$ have been plotted against the applied $V_{G,\,top}$ (see Figure 13: right).

Two linear relationships between $V_{TH}$ and the applied $V_{G,\,top}$ could be observed. These relationships can be explained from the working principles of a dual-gate field-effect transistor that lead to the general equation[26]

$$V_{TH} = -\frac{C_{top}}{C_{bottom}} \cdot V_{G,\,top} \qquad (5)$$

where $C_{bottom}$ is the capacitance of the layer between the active channel and the bottom gate, and $C_{top}$ is that of the layer between the active channel and the top gate. When

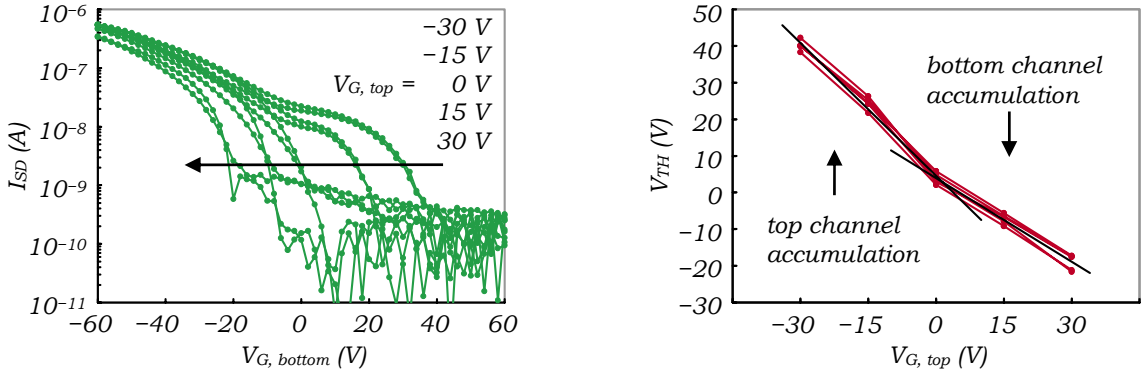


**Figure 13: Threshold voltage shift in a dual-gate field-effect transistor.** *Transfer curves (left) of the MEH-PPV/PMMA dual-gate field-effect transistor (L = 5 µm, W = 20 mm), sweeping $V_{G,\,bottom}$ at different $V_{G,\,top}$ (−30 V, −15 V, 0 V, 15 V and 30 V). A clear shift of $V_{TH}$ can be seen from the graph. $I_{SD}$ has been measured as the current going through the drain electrode at $V_D$ = −2 V. Current leakage to the bottom gate electrode remained below $1\times10^{-7}$ A. Plotting $V_{TH}$ against the applied $V_{G,\,top}$ (right) resulted in a straight line with two slopes. $V_{TH}$ have been plotted in this way for 5 different transistors (right). The average slope of the left part (accumulation only in the top channel) has been determined at −1.12 and the average slope of the right part (accumulation only in the bottom channel) at −0.76. These values were in good agreement with the calculated values of −1.07 and −0.61. All measurements have been performed in vacuum (<$2\times10^{-6}$ mbar).*

accumulation only occurs in the top channel, $C_{bottom}$ will be equal to the capacitance of the bottom insulator ($C_{I,\ bottom}$) and of the semiconductor ($C_S$) in series. $C_{top}$ will simply be the capacitance of the top insulator ($C_{I,\ top}$). Equation 5 now becomes[26]

$$V_{TH} = -\frac{C_{I,\ top} \cdot (C_{I,\ bottom} + C_S)}{C_{I,\ bottom} \cdot C_S} \cdot V_{G,\ top} \qquad (6)$$

Similar reasoning for the case in which accumulation only occurs in the bottom channel results in[26]

$$V_{TH} = -\frac{C_{I,\ top} \cdot C_S}{C_{I,\ bottom} \cdot (C_{I,\ top} + C_S)} \cdot V_{G,\ top} \qquad (7)$$

When $C_S$ is much higher than $C_{I,\ bottom}$ and $C_{I,\ top}$, both Equation 6 and 7 reduce to

$$V_{TH} \approx -\frac{C_{I,\ top}}{C_{I,\ bottom}} \cdot V_{G,\ top} \qquad (8)$$

which is a single linear relationship between $V_{TH}$ and $V_{G,\ top}$, as reported before.[22-25] Here, however, the semiconductor (MEH-PPV) has a similar capacitance as both the insulators (silicon oxide and PMMA). So in this case, both Equation 6 and 7 have to be taken into account, which explains the observed two linear relationships between $V_{TH}$ and the applied $V_{G,\ top}$.

The slopes of the two observed linear relationships between $V_{TH}$ and the applied $V_{G,\ top}$ have been determined from all transistors. The average slope of the left part of the curves (accumulation only in the top channel) has been determined at −1.12 and the average slope of the right part of the curves (accumulation only in the bottom channel) at −0.76. To compare these values with the linear relationships as given in Equation 6 and 7, the capacitance of the different layers had to be calculated. Again, it was assumed that the different (insulator) layers could be approximated by a parallel-plate capacitor, for which the capacitance is given by

$$C = \varepsilon_r \varepsilon_0 \frac{A}{d} \qquad (9)$$

where $\varepsilon_r$ is the dielectric constant of the material, $\varepsilon_0$ is the vacuum permittivity ($8.854\times10^{-12}$ F m$^{-1}$), $A$ is the area and $d$ is the layer thickness. Since the area ends up in both the numerator and denominator in Equation 6 and 7, and therefore cancelling each other, it was sufficient to calculate the capacitance per unit area

$$C = \frac{\varepsilon_r \varepsilon_0}{d} \qquad (10)$$

With its thickness of 300 nm and dielectric constant of 3.9, the silicon oxide layer had a capacitance per unit area of $1.2\times10^{-4}$ F m$^{-2}$. Filling in the values of MEH-PPV ($d$ = 86 nm, $\varepsilon_r$ = 3) resulted in a capacitance per unit area of $3.1\times10^{-4}$ F m$^{-2}$. Similarly, for PMMA ($d$ = 354 nm, $\varepsilon_r$ = 3.6) the capacitance per unit area was calculated at $0.9\times10^{-4}$ F m$^{-2}$. Using these values in Equation 6 (accumulation only in the top channel) and Equation 7 (accumulation only in the bottom channel) resulted in a theoretical slope of −1.07 and −0.61 respectively. Hence, the experimentally obtained slopes are in good agreement with theory.

The data on threshold voltage shifts in the MEH-PPV/PMMA dual-gate field-effect transistor are also part of the publication in *Organic Electronics*.[26]

### 4.1.2. MEH-PPV/P(VDF-TrFE)

The transistors of MEH-PPV/P(VDF-TrFE) have been manufactured on a wafer with 1000 nm silicon oxide. The thickness of the spincoated layers was 50 nm for MEH-PPV and 334 nm for P(VDF-TrFE). The obtained transistors basically lacked typical transistor behaviour. Most transistors did not show OFF-switching, or only very little, and $I_{SD}$ were high and only slightly dependent on $V_G$. If present, ON-switching took place at relative high positive values of $V_G$. Threshold voltage shifts could not be observed due to the bad quality of the transfer curves. It is thought that doping of the semiconductor was the main cause of the observed characteristics due to the relatively long time delay between manufacturing and measuring of these transistors.

### 4.1.3. PAA/PMMA

PAA has been chosen as an alternative semiconductor material, since PAA is known to be stable in air. The transistors of PAA/PMMA have been manufactured on a wafer with 500 nm silicon oxide. The thickness of the spincoated layers was 50 nm for PAA and 345 nm for PMMA. The obtained transistors showed typical transistor behaviour for both the bottom channel and the top channel. At $V_G = -50$ V and $V_D = -20$ V currents were obtained in the ON-state of about $1\times10^{-6}$ A and even nearly $1\times10^{-5}$ A was reached for transistors with $L = 5$ µm and $W = 20$ mm. ON-switching typically occurred around $V_G = -12$ V for the bottom channel and around $V_G = -2$ V for the top channel (see Figure 14: top left). Output curves showed proper linear behaviour at low $V_D$ and saturation at high $V_D$. $I_{SD}$ seemed to be increased with a factor of 10 due to the presence of the silver top gate electrode when comparing dual-gate- and PMMA-coated single-gate field-effect transistors (see Figure 14: top left). A clear reason for this could not be found. Current leakage to the gate electrode remained below $1\times10^{-8}$ A for both the top- and bottom gate electrode.

Sweeping $V_{G,\,bottom}$ at different $V_{G,\,top}$ resulted again in a shift of $V_{TH}$ from positive to negative $V_{G,\,bottom}$ when $V_{G,\,top}$ was increased from negative to positive values (see Figure 14: top right). The typical large shoulder at negative $V_{G,\,top}$, as seen with the MEH-PPV/PMMA dual-gate field-effect transistor, was not observed as clearly here. Also the dependence of $V_{TH}$ on $V_{G,\,top}$ did not clearly show two linear relationships. Only a slight difference in slope in the two parts of the curves and a jump from one regime to the other could be observed (see Figure 14: bottom left). It is thought that this behaviour had to do with the capacitance of the semiconducting layer. Since the semiconducting layer is much smaller than the insulating layers, the capacitance of the semiconducting layer is much higher. Its value is already about 10 times higher when assuming similar dielectric constants, resulting in basically only one linear relationship between $V_{TH}$ and $V_{G,\,top}$. This is supported by the lack of double ON-switching in the transfer curves at negative $V_{G,\,top}$.

The PMMA-coated single-gate transistors, that is, the dual-gate transistors without a silver top gate electrode, were measured also in air at ambient pressure. In air, $V_{TH}$ seemed to be shifted to a more positive value (+3 V) compared to the value in vacuum (see Figure 14: top left). After 30 minutes in air, $V_{TH}$ was shifted even more to almost +15 V and a shoulder, a typical indication of doping,[20] started to appear. Although

$V_{TH}$ was shifted, $I_{SD}$ remained at the same value of about $1\times10^{-6}$ A. In some of the other measurements done in air an even more severe doping behaviour has been observed. Reducing the pressure inside the measurement setup seemed to shift $V_{TH}$ to less positive values again. Therefore, it was concluded that exposing PAA to air does not change its performance irreversibly, although its performance was certainly different in air than it was in vacuum.

It is thought that the shift in $V_{TH}$ was due to doping of the semiconductor by water. Water vapour from the air was probably absorbed by the polymer layers. Since the triarylamine unit in PAA is a base, it can extract a proton from a water molecule. This

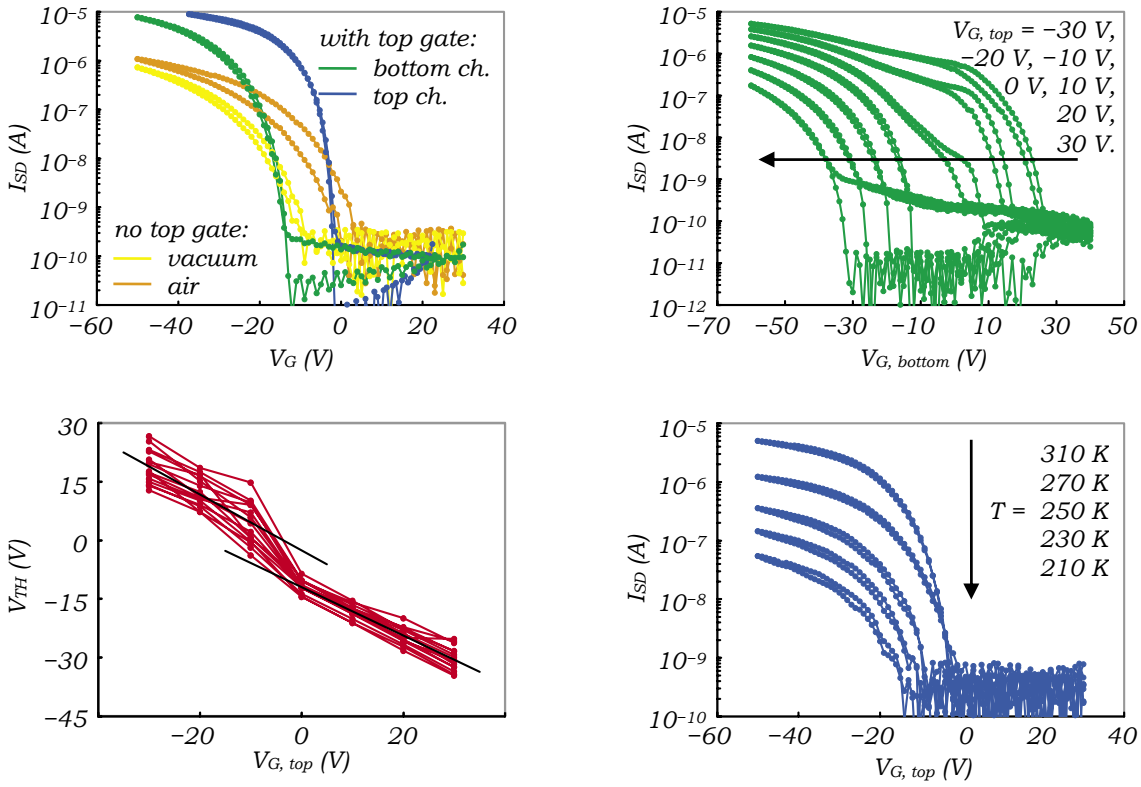


**Figure 14: Transistor characteristics PAA/PMMA.** *Transfer curves (top left) of the PAA/PMMA dual-gate field-effect transistor (L = 5 µm, W = 20 mm) at $V_D$ = −20 V. Curves are plotted of the bottom channel (green) and top channel (blue) in vacuum (<1.5×10⁻⁶ mbar) with top gate electrode present. Also curves are plotted of the bottom channel, without top gate electrode present, in vacuum (yellow) and in air (orange). $V_{G,\,top}$ has been corrected for the difference in capacitance between the bottom- and top isolator. Sweeping $V_{G,\,bottom}$ at different $V_{G,\,top}$ (−30 V, −20 V, −10 V, 0 V, 10 V, 20 V and 30 V) resulted in a shift of $V_{TH}$ (top right). The dependence of $V_{TH}$ on $V_{G,\,top}$, extracted from 15 different transistors, showed only a slight difference in slope in the two parts of the curves and a jump from one regime to the other (bottom left). Transfer curves have also been measured at different temperatures (210 K, 230 K, 250 K, 270 K and 310 K) (bottom right). The depicted curves are of the top channel of an L = 5 µm, W = 20 mm transistor at $V_D$ = −20 V. Current leakage to the top gate remained below 2×10⁻⁸ A. Similar results has been obtained for the bottom channel. All $I_{SD}$ have been measured as the current going through the drain electrode. The dual-gate field-effect transistors have been manufactured at a 500 nm oxide silicon wafer, with Ag top gate electrode. The thickness of the spincoated layers was 50 nm PAA and 345 nm PMMA, and 45 nm PAA and 391 nm PMMA in the case of the temperature measurements.*

proton ends up on the nitrogen atom, which therefore becomes positively charged. Now, the semiconductor layer contains many more positive charges that can freely move along the molecules of the semiconductor. A low positive bottom gate voltage can not deplete the charges from the semiconductor-insulator interface anymore, as it could with the non-doped semiconductor, therefore shifting $V_{TH}$ to positive voltages.
Several dual-gate field-effect transistors have also been measured at different temperatures (see Figure 14: bottom right). A clear dependence on temperature could be observed: the lower the temperature, the lower $I_{SD}$ in the ON-state. Also the $V_{TH}$ was shifted to more negative values at lower temperature. Current leakage to the gate electrodes remained below $2\times10^{-8}$ A. The results were in correspondence with theory, since at lower temperatures the mobility of charge carriers decreases. From the transfer curves at different temperatures the contact resistance has been determined by the transfer line method (TLM).[39] No clear relation between the contact resistance and the temperature could be obtained. Since temperature dependence measurements are not of real importance for sensor behaviour, no further experiments have been carried out related to this.

### 4.1.4. Concluding remarks

From the experiments carried out on dual-gate field-effect transistors it can be concluded that transistors composed of MEH-PPV/PMMA and PAA/PMMA are suitable transistors to be used in a sensor. Two channels were present in the semiconductor layer and both were active. The threshold voltage could be accurately controlled by the second gate electrode, which is crucial for a well working sensor. Also air stability is of importance, since detection usually can not take place in vacuum. PAA was slightly influenced by air, but this influence was not irreversible. PAA still showed reasonably good transistor characteristics and seemed not to be damaged by exposure to air. Therefore, PAA has been chosen as the semiconductor material in further experiments.
In future experiments, other combinations of semiconducting and insulating organic polymers can be studied to search for suitable materials that are not influenced by air. For example, thiophene-based semiconducting polymers that are air stable have been reported.[40] Such polymers are possibly suitable alternatives for PAA and their dual-gate field-effect characteristics should be studied to see whether they are indeed suitable to be used in neuronal signal sensors eventually. More experiments should be carried out, with PAA as well, to study and thoroughly understand transistor characteristics in air.

## 4.2. Water blocking layers

The natural environment of neurons is an aqueous one. Therefore, field-effect transistors used in sensors for detecting and measuring neuronal signals will be in contact with water. To avoid problems, water needs to be blocked from the electrodes in the field-effect transistor. The water blocking capability of PAA, PMMA, P4VP and combinations with crosslinker have been studied systematically.

### 4.2.1. Conduction of water

It is important to know what happens when water is exposed to the currents and voltages present in a field-effect transistor. Therefore, a droplet of water has been placed on a cleaned standard field-effect transistor substrate (silicon, 200 nm silicon oxide, gold interdigitated finger pattern) and the *I-V* characteristics have been measured (see Figure 15: left). The current through the water droplet ($I_{SD}$) started to appear at a voltage ($V_D$) of about −1.9 V. The conductance, that is, the slope of the curve, increased when $V_D$ was lowered below about −3.4 V.

The water used in all experiments was demi water. Demi water does not contain any ions, except for the negligible amount of $H^+$ and $OH^-$ ions due to the dissociation of several water molecules. Hence, virtually no ionic charge carriers are present in demi water, which makes is poorly conducting. This indeed could be seen in the first part of the *I-V* curve where $I_{SD}$ was nearly zero. However, when a large enough voltage difference is applied across a water droplet, non-spontaneous reduction and oxidation reactions can be induced, known as electrolysis.[9] The first reaction that is induced is the break-up of water into hydrogen and oxygen, for which a standard voltage difference of 1.23 V is needed (at 298 K and standard pressure). To obtain a significant rate of this reaction, however, a larger voltage difference is necessary. This is known as the addition of an overpotential.[9] During electrolysis, electrons are extracted from one of the electrodes and added to the other electrode. The actual result is a current that runs from one electrode to the other, which explains the observed increase of $I_{SD}$ below −1.9 V. Also the generation of (gaseous) hydrogen and oxygen has been observed as raising bubbles that appeared in the water droplet at large negative voltage. It was not clear what exactly caused the increase of conductance below −3.4 V. It is thought, however, that this has to be linked to another reaction that can be induced by application of a voltage difference, involving gold and the generation of gold ions.

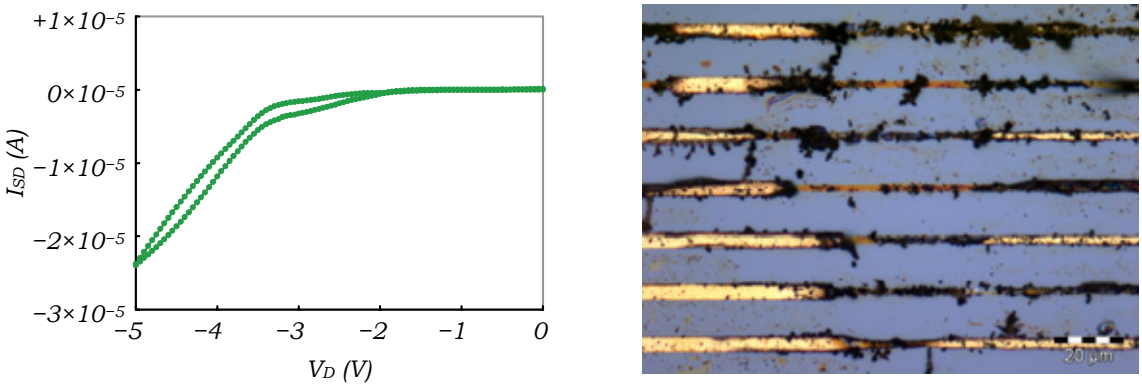


**Figure 15: Electrolysis of water.** *Current-voltage ($I_{SD}$-$V_D$) characteristics of water on a 200 nm oxide standard field-effect transistor substrate for L = 40 µm and W = 10 mm with $V_G$ = 0 V (left). First, $I_{SD}$ was nearly zero, but it started to appear at $V_D$ = −1.9 V due to electrolysis. The conductance increased when $V_D$ was lower than about −3.4 V. The result of electrolysis was a heavily damaged source- and drain electrode (right). Optical image is from a different transistor substrate, which did undergo severe electrolysis too. Scale bar: 20 µm. Optical image taken with an Olympus optical microscope equipped with a Color View Soft Imaging System camera.*

Electrolysis not only led to a significant increase in current, it also damaged the gold source- and drain electrodes (see Figure 15: right). It is thought that the induced reaction involving gold played a part in damaging the electrodes, since it converts solid gold into gold ions. However, since non-spontaneous reactions were induced, a lot of energy was added to the system. It is thought that heat generation and the formation of hydrogen- and oxygen bubbles were the major contributors to the destruction of the electrodes.

Not only the voltage applied between the source- and drain electrodes caused electrolysis. Some of the standard field-effect transistor substrates, with 200 nm silicon oxide, appeared not to be insulating enough. When a droplet of water was applied to those substrates, keeping $V_D$ at sufficiently low voltages, electrolysis was observed. Several tests have been carried out and no surface conduction, for example from a monolayer of water on the surface, was observed. Therefore, the electrolysis and/or the increase in current were not due to surface conduction. Neither did the silicon oxide layer conduct any current when water was not applied to the substrate.

It is thought that the silicon oxide contained leak channels, which could be covered and filled by a droplet of water. The result is a direct contact between the gate electrode, water and the source- and drain electrodes, leading to electrolysis. This idea of leak channels was supported by the observation of bubble formation directly on the silicon oxide layer next to the source- and drain electrodes. Strangely enough, currents only ran from the source- or drain electrode to the gate; to other way around was not observed. Therefore, it seemed like the water-filled leak channels in the silicon oxide acted as a diode. An explanation for this behaviour could not be given and was also beyond the scope of the work done here.

In general, it turned out that on the standard field-effect transistor substrates a 200 nm silicon oxide layer shielded the underlying silicon from water only on some substrates. It is thought that this could be linked to the quality of the silicon oxide layer, which might have been higher at substrates originating from the centre of the 6-inch inch wafer than at substrates originating more from the edge. A 2000 nm silicon oxide layer shielded the underlying silicon from water in every case, irrespective of the location of the substrate in the 6-inch wafer.

### 4.2.2. Water blocking capability of PAA

To avoid obtaining large $I_{SD}$ due to electrolysis and thereby damaging the electrodes, $V_D$ and $V_G$ should be kept at values between 0 V and −1.9 V. However, PAA field-effect transistors had a typical $V_{TH}$ much more negative than −1.9 V. Moreover, to obtain high $I_{SD}$ in the ON-state and clear ON-switching, also $V_D$ needed to be more negative than −1.9 V (see again Figure 12: left). In order to use large negative $V_G$ and $V_D$, without electrolysis occurring, water had to be blocked from both the gate electrode and the source- and drain electrodes to avoid any contact between water and the electrodes.

It was tested whether a layer of PAA was water blocking. This was tested on a standard field-effect transistor substrate with properly insulating silicon oxide to avoid influence from the gate electrode. The current-voltage ($I_{SD}$-$V_D$) characteristics showed similar behaviour as when the water droplet was placed on a bare substrate (see

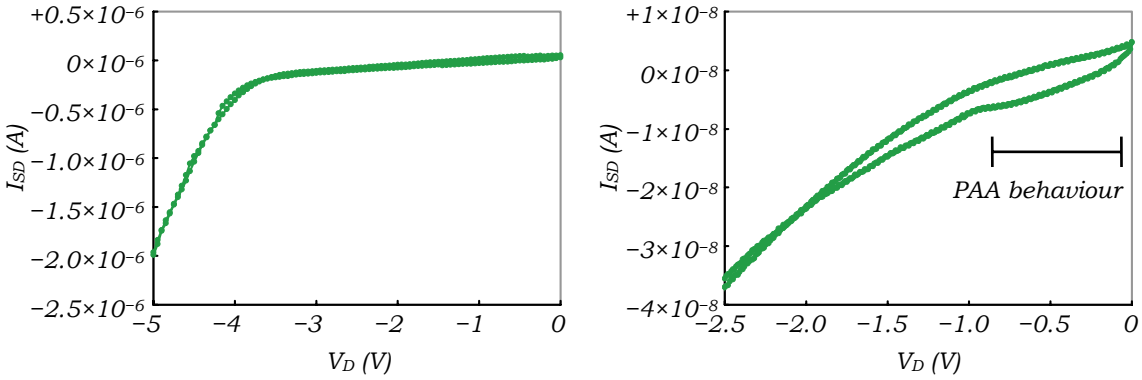


**Figure 16: Water on PAA.** *Current-voltage ($I_{SD}$-$V_D$) characteristics of water on a 200 nm oxide standard field-effect transistor substrate with PAA for L = 40 µm and W = 10 mm with $V_G$ = −5 V (left). It showed the same behaviour as when water was placed on a bare substrate (see Figure 15: left). It is clear that electrolysis took place and that PAA was not water blocking. Only at very low $V_D$ the behaviour of PAA could be observed (right). The thickness of the spincoated layer of PAA was about 80 nm.*

Figure 16: left and compare with Figure 15: left). It was clear that electrolysis took place and that PAA was not water blocking. Only at very low $V_D$ the behaviour of PAA could be observed (see Figure 16: right), since in this regime the conduction of water was lower than the conduction of PAA.

### 4.2.3. Water blocking capability of PMMA

Since the semiconductor layer of PAA was not water blocking, the water blocking capability of several insulators has been studied systematically. First, a definition was formulated when to consider a layer of material as water blocking.

For the water blocking experiments, the transfer characteristics, that is, $I_{SD}$ versus $V_G$, has been studied. In general, when there was no difference between the transfer curves with and without a droplet of water, the transistor was said to be blocked from water. More specifically, on a bare standard field-effect transistor substrate this meant that no ON-OFF switching was observed and $I_{SD}$ remained constant, preferably below $5\times10^{-9}$ A, but at least below $2\times10^{-8}$ A, at $V_G$ between −20 V and +20 V. If PAA was present on the substrates, this meant that similar ON-OFF switching was observed as without water, that is, $I_{SD}$ was not constant between $V_G$ = −20 V and +20 V, and that $I_{SD}$ in the ON-state did not reach values above $5\times10^{-5}$ A. In addition, for any case, formation of bubbles inside the water droplet was not allowed to occur. Additional support for no change of $I_{SD}$ was sometimes obtained from measuring $I_{SD}$ over time while applying a water droplet. When the majority of the total number of transistors measured, with a certain insulator layer, was marked as blocked from water, then this typical insulator layer was said to be water blocking.

Several PMMA layers of different thicknesses have been studied. A summary of all the results is given in Table 2. It demonstrates that PMMA was water blocking when the layer was 996 nm or more. A top insulator of this thickness, however, is not ideal for the dual-gate transfer characteristics. Since the layer is relatively thick, a large voltage

has to be applied on the top gate to effectively influence the charge carriers and conduction channels in the semiconductor layer. This is especially a disadvantage when putting it in the context of a sensor, since a high top gate voltage is translated into a lot of analyte necessary to influence the transfer characteristics. Therefore, a thick top insulator increases the detection limit and decreases the sensitivity of a sensor.

To decrease the layer thickness of PMMA that was sufficient to make it water blocking, a crosslinker has been added to PMMA. Typically, a crosslinker reacts with the polymer and/or itself, creating a dense network of crosslinked polymer or crosslinker material. Such a dense network is likely to perform better in blocking of water than a regular polymer network. Many crosslinkable polymers are known that are good thin insulators. A drawback of most of these, however, is their need for a high annealing temperature, which would damage the underlying PAA. To overcome this problem, the crosslinker 1,6-bis(trichlorosilyl)hexane has been used. Crosslinking of this crosslinker already takes place at moderate temperatures in the presence of oxygen and moisture in air.[41,42] Moreover, layers of PMMA crosslinked with this crosslinker have been reported as good (electrical) insulators down to a thickness of about

**Table 2: Water blocking capability of PMMA.** *Summary of all experiments carried out to study the water blocking capability of PMMA layers. Both the number of water blocking transistors of the total number of transistors measured (#/#) and the conclusion whether the layer was water blocking ('yes' or 'no') are given in the table. Some remarks are placed in the last column. PMMA dissolved in either MEK or butylacetate and PMMA e-beam photoresist have been tested. All PMMA+crosslinker are annealed in air.*

| *Material* | *Thickness* | *Water blocking* | | *Remarks* |
|---|---|---|---|---|
| *PMMA* | *38 nm* | *0/4* | *no* | *Dissolved in butylacetate* |
| *PMMA* | *56 nm* | *0/4* | *no* | *Dissolved in butylacetate* |
| *PMMA e-beam* | *69 nm* | *0/3* | *no* | *On 80 nm PAA, annealed in $N_2$ at 120 °C* |
| *PMMA e-beam* | *113 nm* | *0/1* | *no* | *On 80 nm PAA, annealed in $N_2$ at 120 °C* |
| *PMMA* | *187 nm* | *0/4* | *no* | *Annealed in air* |
| *PMMA* | *220 nm* | *0/4* | *no* | |
| *PMMA* | *377 nm* | *2/4* | *no* | *Annealed in air, $I_{SD}$ constant at $3\times10^{-8}$ A* |
| *PMMA* | *544 nm* | *0/1* | *no* | |
| *PMMA* | *593 nm* | *1/4* | *no* | *$I_{SD}$ constant at $2\times10^{-8}$ A* |
| *PMMA* | *682 nm* | *1/4* | *no* | *Annealed in air* |
| *PMMA* | *996 nm* | *3/4* | *yes* | |
| *PMMA* | *1625 nm* | *3/4* | *yes* | *$4^{th}$ transistor leaking due to hole in PMMA layer* |
| *PMMA* | *2313 nm* | *4/4* | *yes* | |
| *PMMA* | *3057 nm* | *4/4* | *yes* | |
| *PMMA* | *5700 nm* | *3/3* | *yes* | |
| *PMMA+crossl.* | *272 nm* | *2/4* | *no* | *$I_{SD}$ constant at $4\times10^{-8}$ A* |
| *PMMA+crossl.* | *493 nm* | *4/4* | *yes* | *1 transistor $I_{SD}$ constant at $3\times10^{-8}$ A* |
| *PMMA+crossl.* | *840 nm* | *4/4* | *yes* | |

50 nm.[42] Therefore, this crosslinker was thought to be a suitable candidate for obtaining a thinner water blocking PMMA layer.
Several layers of PMMA mixed with the crosslinker have been studied, all with a different layer thickness. A summary of these results is also given in Table 2, which shows that PMMA mixed with the crosslinker was water blocking when the layer was 493 nm or more. Therefore, the minimum insulator layer thickness required to block the electrodes from water had been reduced by 500 nm, simply by addition of the crosslinker to PMMA.

### 4.2.4. Influence of crosslinker on PAA characteristics

Dual-gate and coated single-gate field-effect transistors have been manufactured, with PMMA mixed with crosslinker as the top insulator and coating layer respectively, to study the influence of this water blocking layer on PAA. Transfer curves showed behaviour corresponding to highly doped PAA (see Figure 17). Especially the coated single-gate field-effect transistor did not show much ON-OFF switching anymore and $I_{SD}$ in the 'ON'-state was almost a factor 10 larger than in the case of PMMA without crosslinker. Moreover, the dual-gate field-effect transistor showed that the top channel was much more doped than the bottom channel, as seen by the large shift in threshold voltage. Therefore, it was concluded that the crosslinker was the origin of the doping of PAA.

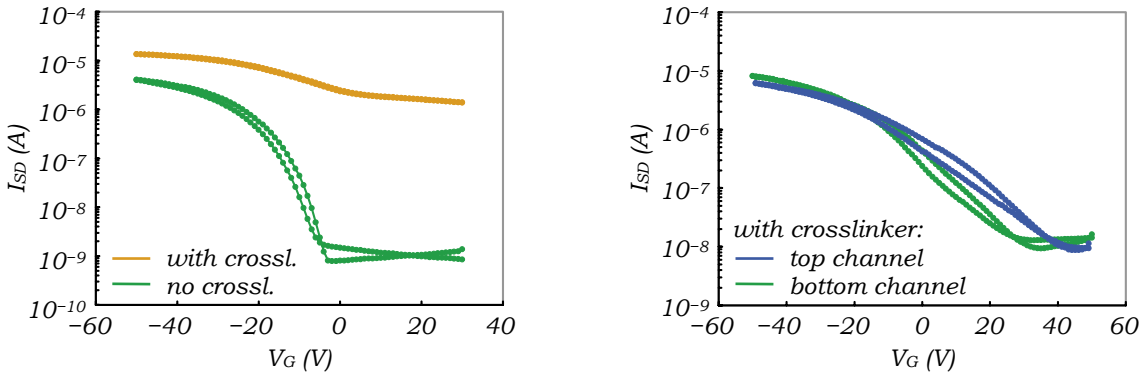


**Figure 17: Influence of crosslinker on transfer characteristics PAA.** *Transfer characteristics of PAA in a dual-gate (right) and coated single-gate (left) field-effect transistor (L = 5 µm, W = 10 mm), with PMMA mixed with crosslinker as the top insulator and coating layer respectively, as measured in vacuum (<1.5×10⁻⁶ mbar). $I_{SD}$ have been measured at $V_D$ = −20 V as the current going through the drain electrode. Addition of the crosslinker resulted in typical doping behaviour of PAA (left: orange) with severely reduce ON-OFF switching compared to the case without crosslinker (left: green). The top channel (right: blue) was more influenced by the crosslinker than the bottom channel (right: green). $V_{G,\,top}$ has been corrected for the difference in capacitance between the bottom- and top isolator. In all cases, current leakage to the gate electrode remained below 3×10⁻⁷ A. The coated single-gate field-effect transistor has been manufactured on a 200 nm oxide standard field-effect transistor substrate and the thickness of the spincoated layers was 77 nm PAA and 186 nm PMMA (no crosslinker), and 72 nm PAA and 228 nm PMMA+crosslinker. The dual-gate field-effect transistor has been manufactured at a 300 nm oxide silicon wafer, with Ag top gate electrode. The thickness of the spincoated layers was 59 nm PAA and 427 nm PMMA+crosslinker.*

This conclusion can be explained by looking at what happens when crosslinking occurs. When the crosslinker reacts, under influence of water in the air, HCl is produced. As explained before, PAA is basic, so it will act as a strong scavenger for the HCl produced by the crosslinking process. The result is a proton on the nitrogen atom of PAA, leading to an increase of positive charge carriers in the semiconductor material and, therefore, to a shift of $V_{TH}$ to (very large) positive voltages. Indeed, this has been observed in the transfer characteristics of the field-effect transistors. The difference in degree of doping between the bottom- and top channel supported the idea that the dopant, HCl in this case, originated from the crosslinker in the insulator layer.
The PAA in the dual-gate field-effect transistor was less doped than the PAA in the coated single-gate field-effect transistor. This was due to the fact that the dual-gate field-effect transistor had not been annealed. Therefore, the crosslinking reaction had not been taken place at the same scale as in the coated single-gate field-effect transistor, so the amount of HCl produced was far less. Nevertheless, it was enough to dope the PAA to some extent and to demonstrate the difference in doping between the bottom- and top channel.

### 4.2.5. P4VP as HCl scavenger

To avoid doping of PAA, a basic insulator material was used that would act as a scavenger for the HCl formed by the crosslinking reaction. P4VP was proposed as a suitable material, since it contains a nitrogen atom capable of receiving a proton.
A coated single-gate field-effect transistor similar to the ones before has been manufactured. In this case, P4VP has been used as the coating layer. Addition of crosslinker to the P4VP solution, however, resulted in an immediate reaction between P4VP and the crosslinker to an insoluble substance. Therefore, it was not possible to manufacture a coated single-gate field-effect transistor with a coating layer made out of P4VP mixed with crosslinker. Nevertheless, transistors have been made with only P4VP as the coating layer and these transistors showed exactly the same behaviour as transistors with only PMMA as the coating layer. This has also been expected, since the PAA layers were equal and no doping agents were present.
To still include the crosslinker in the coating layer, the crosslinker was spincoated from a 5% mixture with MEK as a separate layer on top of P4VP. The layer was annealed in a nitrogen atmosphere, without water, in order to let the crosslinker react with P4VP instead of with itself. The transfer characteristics of this coated single-gate field-effect transistor, with P4VP/crosslinker as the coating layer, were highly comparable to the characteristics of a coated single-gate field-effect transistor with only P4VP as the coating layer (see Figure 18: left). No doping of PAA has been observed, so it was concluded that P4VP acted as a good scavenger for the HCl produced during the crosslinking reaction and that it completely blocked the HCl from entering PAA.
Also coated single-gate field-effect transistors have been manufactured with crosslinker spincoated on top of P4VP from 10%, 50% and 100% mixtures with MEK. The layers were first annealed in a nitrogen atmosphere, in order to let the crosslinker react with P4VP. Subsequently, the layers were annealed in air, to let any remaining crosslinker react with itself. The obtained coated single-gate field-effect transistors

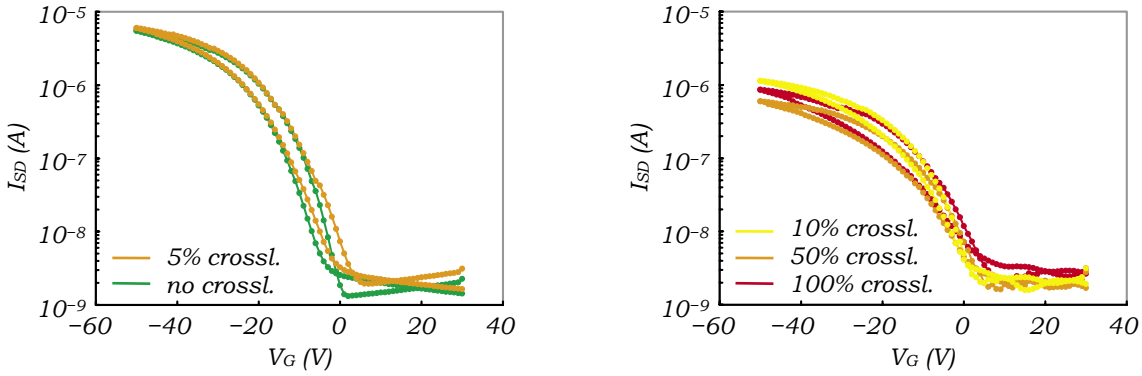


**Figure 18: P4VP as HCl scavenger.** *Transfer characteristics of PAA in a coated single-gate field-effect transistor with P4VP/crosslinker as the coating layer. Spincoating the crosslinker, from a 5% mixture with MEK, on top of P4VP did not result in doping behaviour of PAA (left) (orange), but gave similar behaviour as without crosslinker on top (green). Spincoating the crosslinker from more concentrated mixtures (right), that is, 10% (yellow), 50% (orange) and 100% (red), resulted in similar transfer characteristics, although with a slight shift of $V_{TH}$, indicating some doping of PAA. In all cases, current leakage to the gate electrode remained below $2\times10^{-7}$ A. $I_{SD}$ have been measured at $V_D = -20$ V as the current going through the drain electrode on an $L = 5$ µm, $W = 10$ mm transistor (P4VP and P4VP/5% crosslinker), and on an $L = 20$ µm, $W = 10$ mm transistor (P4VP/5%,10%,100% crosslinker). Measurements were performed in vacuum, that is, $<1.1\times10^{-6}$ mbar for P4VP and P4VP/5% crosslinker, and $<8\times10^{-6}$ mbar for P4VP/5%,10%,100% crosslinker. The coated single-gate field-effect transistors have been manufactured on 200 nm oxide standard field-effect transistor substrates. The thickness of the spincoated layers was 79 nm PAA, 231 nm P4VP (no crosslinker on top), 316 nm P4VP/5% crosslinker, 435 nm P4VP/10% crosslinker, 938 nm P4VP/50% crosslinker and 506 nm P4VP/100% crosslinker.*

showed similar transfer characteristics as the ones with only P4VP and P4VP/5% crosslinker as the coating layer (see Figure 18: right). However, $V_{TH}$ was slightly shifted to positive values, indicating some doping of PAA. It seemed like 100% crosslinker spincoated on top of P4VP induced the most doping in PAA. Apparently, P4VP was only capable of acting as a scavenger up to a certain amount of HCl. When too much crosslinker was present, too much HCl was produced and part of it could still dope PAA, despite the presence of the scavenger layer in between.

All different coating layers based on P4VP have also been tested for their water blocking capability. A summary of the results of these measurements is given in Table 3. Unfortunately, none of the studied layers turned out to be water blocking. However, since P4VP acted as a blocking layer for HCl when the crosslinker was spincoated directly on top of it, it was suggested that P4VP could also block HCl formed in a layer of PMMA mixed with crosslinker. Since PMMA mixed with crosslinker was water blocking down to 500 nm, a combination of P4VP, PMMA and the crosslinker could result in a water blocking layer, without doping the semiconductor layer.

Coated single-gate field-effect transistors, therefore, have been manufactured with a coating layer consisting of spincoated P4VP followed by a spincoated mixture of PMMA with crosslinker. The transistors were annealed in air in order to let the crosslinker react with itself. Three different layer thicknesses of P4VP (15 nm, 68 nm and 206 nm)

**Table 3: Water blocking capability of P4VP.** *Summary of all experiments carried out to study the water blocking capability of layers involving P4VP. Both the number of water blocking transistors of the total number of transistors measured (#/#) and the conclusion whether the layer was water blocking ('yes' or 'no') are given in the table. Some remarks are placed in the last column. PMMA+crosslinker layer was 353 nm thick.*

| *Material* | *Thickness* | *Water blocking* | | *Remarks* |
|---|---|---|---|---|
| *P4VP* | *245 nm* | *0/1* | *no* | *On 77 nm PAA* |
| *P4VP/5% crossl.* | *316 nm* | *0/1* | *no* | *On 79 nm PAA, annealed in $N_2$* |
| *P4VP/10% crossl.* | *435 nm* | *0/1* | *no* | *On 80 nm PAA, annealed in $N_2$ and air* |
| *P4VP/50% crossl.* | *938 nm* | *0/1* | *no* | *On 80 nm PAA, annealed in $N_2$ and air* |
| *P4VP/100% crossl.* | *506 nm* | *0/1* | *no* | *On 80 nm PAA, annealed in $N_2$ and air* |
| *P4VP/PMMA+crossl.* | *15 nm* | *0/1* | *no* | *On 87 nm PAA, annealed in air* |
| *P4VP/PMMA+crossl.* | *68 nm* | *0/1* | *no* | *On 87 nm PAA, annealed in air* |
| *P4VP/PMMA+crossl.* | *206 nm* | *0/1* | *no* | *On 87 nm PAA, annealed in air* |

have been used and the transfer characteristics of the resulting coated single-gate field-effect transistors have been measured (see Figure 19). The transistors with the thinnest layer of P4VP showed a large shoulder and a shift of $V_{TH}$ to very positive values, therefore indicating quite some doping. The second thinnest layer of P4VP seemed to block PAA from doping a lot more, as seen from the lower $V_{TH}$, the less apparent shoulder and the lower $I_{SD}$ in the ON-state. The thickest layer of P4VP resulted in $V_{TH}$ shifted to even more negative values, but still a tiny shoulder seemed to be present. Also $I_{SD}$ in the ON-state was not only much lower than in the other two situations, but also about a factor 10 lower than expected for non-doped PAA. From the results, it seemed that a reasonably thick layer of P4VP could block HCl from the PMMA+crosslinker layer. A concrete conclusion, however, could not be extracted from these results, since they did not show sufficiently clear transfer characteristics.
The different combinations of coating layers have also been tested for their water blocking capability. A summary of the results of these measurements is given in Table 3 as well. None of the studied layers turned out to be water blocking. It was thought that this had to do with the layer thickness of the PMMA layer, which was only 353 nm. This layer was probably too thin to be water blocking. Also the extra layers of P4VP could not prevent water from penetrating through the coating layer and getting in contact with the source- and drain electrodes.

### 4.2.6. Concluding remarks

Since electrolysis occurs when water is exposed to the currents and voltages present in the field-effect transistors used, it is important to block water from the electrodes to avoid any contact between them. From the experiments carried out it can be concluded that PMMA was water blocking when its thickness was at least 1000 nm. Adding a crosslinker decreased this lower limit down to 500 nm. However, due to the crosslinking reaction that occurs, the semiconductor layer became doped by HCl. To avoid doping of PAA, the insulator P4VP could be used as an HCl scavenger, which

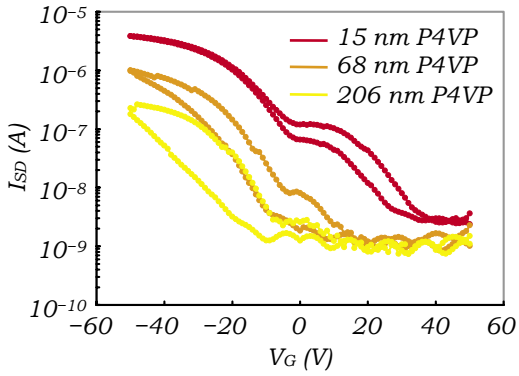


**Figure 19: Blocking of HCl by P4VP.** *Transfer characteristics of PAA in a coated single-gate field-effect transistor (L = 10 µm, W = 10 mm) with P4VP/PMMA+crosslinker as the coating layer. Curves are plotted for a P4VP layer thickness of 15 nm (red), 68 nm (orange) and 206 nm (yellow). The thickest layer of P4VP seemed to block HCl almost entirely, as seen from the very small shoulder and least positive value of $V_{TH}$. However, $I_{SD}$ in the ON-state was about a factor 10 lower than expected for non-doped PAA. Current leakage to the gate electrode generally remained below $1\times10^{-7}$ A. $I_{SD}$ have been measured in vacuum (<$9.5\times10^{-6}$ mbar) at $V_D$ = −20 V as the current going through the drain electrode. The coated single-gate field-effect transistors have been manufactured on 200 nm oxide standard field-effect transistor substrates. The thickness of the spincoated layers was 87 nm PAA and 353 nm PMMA+crosslinker.*

appeared to be successful to a certain extent. So far, the insulating layer structures containing P4VP that have been studied showed no water blocking capability. The use of P4VP as a blocking layer for HCl, placed between the layer of PMMA with crosslinker and the semiconductor layer, seemed to be promising. The resulting relatively large total thickness of the top insulator, however, is again a disadvantage when this transistor will be used in a sensor device.

In future experiments, other top insulator layers can be studied for their water blocking capability, in order to obtain a water blocking layer as thin as possible. Many different insulating polymers are known, like polystyrene, that are good gate insulators in organic field-effect transistors.[43,44] Some of these insulating polymers might also have good water blocking capabilities. Also photoresist materials, like SU-8, might be good water blocking materials, since such materials can be highly crosslinked. The use of a strongly hydrophobic material as the insulator might also work well. To avoid spincoat problems with (slightly) hydrophilic semiconductors and repelling interactions in aqueous environments, the top of these hydrophobic insulators can be hydrophilized by short (~30 seconds) exposure to UV-ozone. Another possibility is to manufacture a multilayer stack of different thin insulating polymers, with the hydrophobic material in the middle of the stack, as such shielding this layer from the aqueous environment. Not only the insulator material can be changed, also many alternative crosslinkers are available on the market. A suitable crosslinker will crosslink at moderate temperatures and does not generate any products that can dope the semiconductors. Otherwise, again, a suitable scavenger or blocking layer for those products has to be found. First, however, the blocking capability of P4VP for HCl should be studied more thoroughly. Also, it might be worth trying to find another HCl

scavenger to use as a blocking layer. In the end, a multilayer top insulator might be developed containing a shielded hydrophobic layer mixed with a suitable crosslinker on top of a scavenger for any doping agents produced by the crosslinker. Finally, some work should be done with respect to the silicon oxide layer on the substrates. A 2000 nm silicon oxide layer requires very high gate voltages to induce ON-OFF switching in the semiconductor, due to the low capacitance of the silicon oxide layer. Substrates with 200 nm silicon oxide are a lot more suitable for use in neuronal signal sensors, since they require much lower gate voltages. Therefore, some work should be done on obtaining good 200 nm silicon oxide layers by, for example, some kind of surface treatment.

## 4.3. Influence of salt solutions

Essential for neurons to survive on top of the field-effect transistor is an aqueous environment with certain specific ingredients. Essential ingredients are NaCl, KCl, $CaCl_2$, $MgCl_2$, glucose and a pH buffering agent. Therefore, the influence of water and solutions of NaCl and KCl on the field-effect transistor characteristics has been studied. In order to study this systematically, a flow channel setup was developed to supply solutions to the transistors in a standard, defined way.

### 4.3.1. Influence of water and NaCl(aq) droplets

To study the influence of water and NaCl(aq) droplets on the transistor characteristics, coated single-gate field-effect transistors have been manufactured with a thick layer of PMMA (946 nm) to block water from contacting the electrodes. In vacuum, transfer characteristics have been measured typical for PAA (see Figure 20: top left). After exposure to air for 2 hours, $V_{TH}$ had been shifted a little to a less negative value and $I_{SD}$ in the ON-state had been slightly increased, so almost no difference was observed between vacuum and exposure to air. When a water droplet was applied on top of the transistors, the transfer characteristics did not change much either. Only hysteresis of the curve was more apparent, but $V_{TH}$ and $I_{SD}$ were similar as before.
Droplets of different solutions of NaCl (1 mM, 10 mM, 100 mM and 1000 mM) in water were also applied on top of the transistors. The transfer curves of PAA in all these cases were equal to the transfer curve when water was applied. Moreover, all transfer curves exactly overlapped each other (see Figure 20: top right). The $I_{SD}$ has also been measured over time to study its behaviour during application and removal of the droplets (see Figure 20: bottom left). None of the solutions caused a severe change in $I_{SD}$. Only the moment of application and removal could be observed as a slight jump and/or peak in current. These changes were, however, very small and did not disturb the general behaviour of the current, which was stabilizing to a certain value.
From the results, it could be concluded that droplets of NaCl(aq) on top of the coated single-gate field-effect transistor did not influence the transfer characteristics of PAA. However, it had to be taken into account that the PMMA layer was relatively thick. Therefore, it could be that the capacitance of this coating layer and top insulator was simply too low for these NaCl solutions to influence the conduction channel in PAA.

Moreover, a lot of salt remained behind on the surface when the droplets of salt solutions were removed (see Figure 20: bottom right). This salt could have influenced subsequent measurements.

### 4.3.2. Influence of NaCl(aq) and KCl(aq): using the flow channel setup

When applying droplets of salt solutions to the surface, it was unavoidable that some salt remained on the surface after removal of the droplets. Therefore, the flow channel setup has been developed. By using this flow channel setup, with a channel in the PDMS block, fluids could be applied to the transistor surface in a standard, defined

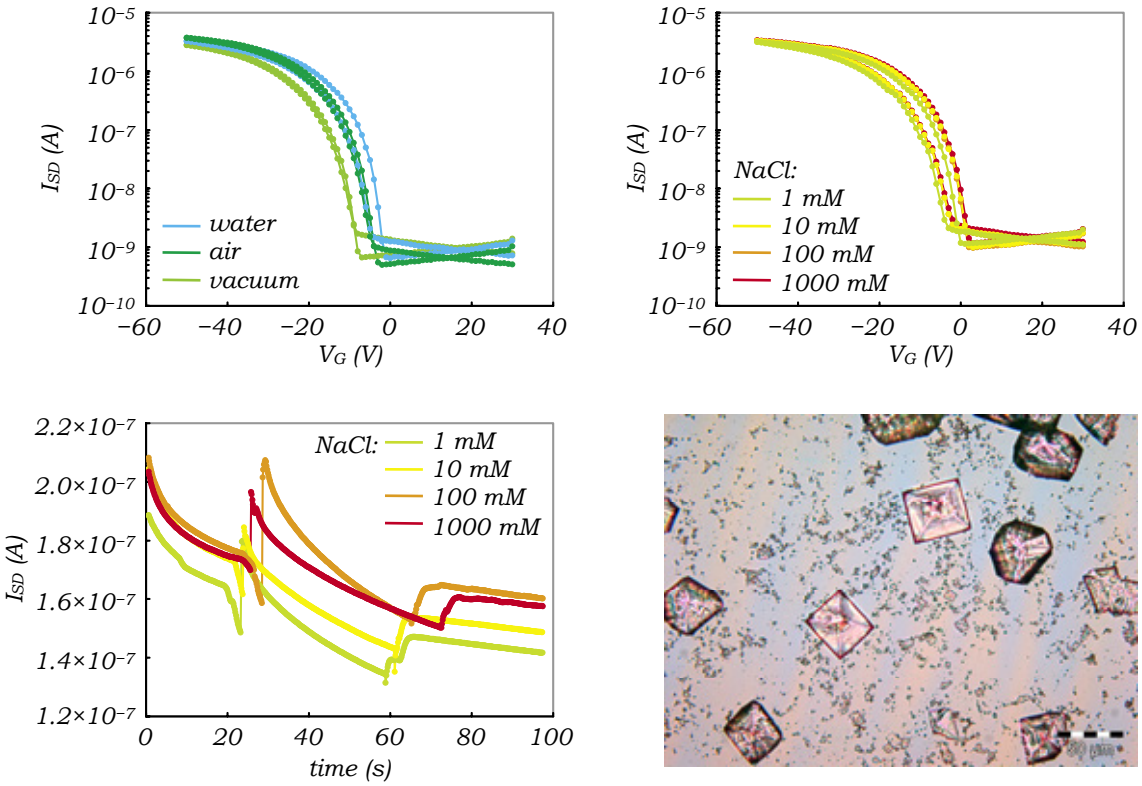


**Figure 20: Influence of water and NaCl(aq) droplets.** *Transfer characteristics of PAA in a coated single-gate field-effect transistor (L = 10 µm, W = 10 mm) with PMMA as the coating layer (top left). Curves are plotted for measurements carried out in vacuum (<2×10⁻⁶ mbar) (light green), after 2 hours exposure to air (dark green) and when a water droplet was applied on top of the transistor (light blue). Also the influence of NaCl(aq) on the transfer characteristics has been studied (top right) by applying droplets of NaCl solutions of 1 mM (yellow green), 10 mM (yellow), 100 mM (orange) and 1000 mM (red). No major changes in any of the transfer curves have been observed. Also measuring $I_{SD}$ over time during application of the droplets did not show any severe changes in $I_{SD}$ (bottom left). After removal of the droplets, NaCl crystals remained on the surface (bottom right). Scale bar: 50 µm. $I_{SD}$ have been measured as the current going through the drain electrode at $V_D = -20$ V (transfer curves), and at $V_D = -2$ V and $V_G = -20$ V ($I_{SD}$ over time). All current leakage to the gate electrode remained below $1\times10^{-7}$ A. The coated single-gate field-effect transistors have been manufactured on a 200 nm oxide standard field-effect transistor substrate. The thickness of the spincoated layers was 45 nm PAA and 946 nm PMMA. Optical image taken with an Olympus optical microscope equipped with a Color View Soft Imaging System camera.*

way (see again Figure 11). Moreover, the surface could be easily rinsed with demi water to remove any remaining salt. In this way, the influence of salt solutions on the transistor characteristics could be studied more systematically than by the droplet method. The PDMS block did not influence the current characteristics of the transistors in any way, as tested by measuring transfer curves with and without PDMS block.

Several coated single-gate field-effect transistors have been manufactured, with PMMA acting as the coating layer and top insulator, with different bottom- and top insulator thicknesses. The transfer characteristics demonstrated that the presence of water did not influence the transistor. Subsequent application of NaCl and KCl solutions did not induce any extra changes (see Figure 21: left). Also $I_{SD}$ did not change significantly over time when applying successively all different solutions (see Figure 21: right). Similar results have been obtained for all transistors, with either a thin (171 nm) or thick (762 nm) layer of PMMA, manufactured on substrates with either 200 nm or 2000 nm silicon oxide. With some transistors, again electrolysis occurred, due to the quality of the 200 nm silicon oxide layers and due to slow penetration of water through the thick PMMA layer. Therefore, on some transistors the full series of solutions could not be tested, since once electrolysis occurred subsequent measurements were not representative anymore. The solutions measured without electrolysis occurring, however, all showed the same result. Therefore, it could be

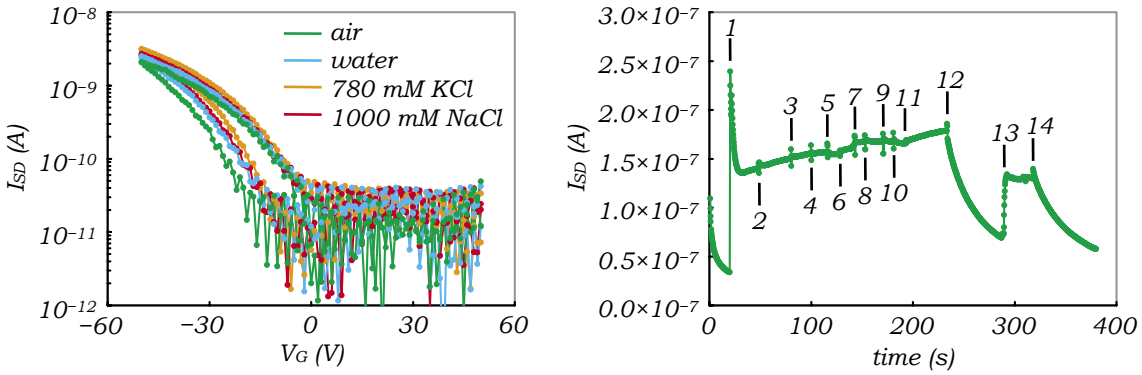


**Figure 21: Influence of NaCl and KCl solutions.** *Transfer characteristics of PAA in a single-gate field effect transistor (L = 40 µm, W = 10 mm) with PMMA as the top insulator, measured at $V_D$ = −1 V (left). Curves are plotted for measurements performed in air (green) and when water (light blue), 780 mM KCl (orange) or 1000 mM NaCl (red) were applied on top of the transistor using the flow channel setup. No difference between the curves has been observed. Also measuring $I_{SD}$ over time, at $V_D$ = −20 V and $V_G$ = −150 V on an L = 10 µm, W = 10 mm transistor, during application of the solutions did not show any severe changes in $I_{SD}$ (right). Indicated are, from (1) to (11), application of water, 1 mM NaCl, 10 mM NaCl, 100 mM NaCl, 1000 mM NaCl, water, 0.78 mM KCl, 7.8 mM KCl, 78 mM KCl, 780 mM KCl and water. At (12) all solutions were removed and $I_{SD}$ was measured in air again. At (13) some water flowed back from the reservoirs in the PDMS block into the channel by capillary forces. At (14) this water was removed again. In all cases, $I_{SD}$ have been measured as the current going through the drain electrode. The single-gate field-effect transistors have been manufactured on 200 nm (transfer curve) or 2000 nm ($I_{SD}$ over time) oxide standard field-effect transistor substrates. The thickness of the spincoated layers was 83 nm PAA and 171 nm (transfer curve) or 762 nm ($I_{SD}$ over time) PMMA.*

concluded that neither water nor NaCl or KCl solutions, with concentrations up to 1 M and 0.78 M respectively, influenced the current characteristics of the coated single-gate field-effect transistors at all.
The observed behaviour could be explained by looking at the nature of the solutions. Although salt solutions contain free ions, each ion is balanced by its counter ion. The result is that any salt solution effectively is neutral and uncharged. Therefore, the salt solutions can not induce any change in the conduction channel of the semiconductor, which indeed has been seen in the measurements.

### 4.3.3. Concluding remarks

From the experiments carried out, it can be concluded that the single-gate field-effect transistor characteristics of PAA, coated with PMMA, are not influenced by either water or solutions of NaCl or KCl. The aqueous environment essential for neurons to survive on top of a field-effect transistor is, therefore, not likely to cause any interference with the transistor. Although generation of an action potential also involves sodium and potassium, ions move across the plasma membrane of the neuron in such a way that a potential is created on the in- and outside of the membrane. Therefore, an excess of positively or negatively charged ions will be present, without their respective counter ions. These excess charges, rendering the local environment positively or negatively charged, are the charges that will influence the conduction channel of a field-effect transistor in a neuronal signal sensor.
In future experiments, also solutions of $CaCl_2$ and $MgCl_2$ should be studied to verify that they will not influence the transistor characteristics. Also solutions of glucose have to be studied. Next, experiments should be carried out to determine the influence of buffer solutions with different pH. When all of this is studied and understood, the next steps can be taken on the way of measuring on neurons.

# 5. Conclusion

The work described here is a first step towards a new type of sensor to detect and measure neuronal signals, based on polymeric dual-gate field-effect transistors. The results obtained show the suitability of these transistors for use in neuronal signal sensors.

## 5.1. Conclusions

Different combinations of semiconducting and insulating organic polymers have been studied for their dual-gate field-effect transistor characteristics. Transistors composed of MEH-PPV/PMMA and PAA/PMMA appeared to be suitable transistors for use in a sensor. Two active channels were present in the semiconductor layer and the threshold voltage could be accurately controlled by the second gate electrode, which is crucial for a well working sensor. The transistor characteristics of PAA were slightly influenced by air, but the material seemed not to be damaged by exposure to air.
Many experiments have been carried out in order to obtain water blocking insulator layers to avoid contact between water and the transistor electrodes, which would lead to electrolysis. PMMA was water blocking when its thickness was at least 1000 nm. Adding a crosslinker decreased this lower limit down to 500 nm. Due to the crosslinking reaction, however, the semiconducting PAA layer became doped by HCl. P4VP was used as an HCl scavenger and -blocking layer to avoid doping of PAA. The studied insulator layer structures with P4VP, however, were not water blocking.
Essential for neurons to survive on top of the field-effect transistor is an aqueous environment with at least NaCl and KCl. Experiments have been carried out to study the influence of water and these salts on the transistor characteristics in a systemic way by using a flow channel setup. The single-gate field-effect transistor characteristics of PAA, coated with PMMA, were not influenced by either water or solutions of NaCl or KCl. It was therefore concluded that the aqueous environment essential for neurons to survive on top of a field-effect transistor is not likely to cause any interference with the transistor.

## 5.2. Future work

In future experiments, the dual-gate field-effect transistor characteristics of other semiconducting polymers should be studied for the air stability of these polymers and for the suitability of these polymers to be used in neuronal signal sensors. Also more experiments have to be carried out to thoroughly understand the transistor characteristics of PAA in air.
To optimally block water from the transistor electrodes, other top insulator layers should be studied. Other insulating polymers can be used, but photoresist materials

and different crosslinkers might be studied for their water blocking capabilities as well. Using a strongly hydrophobic material might also be successful to obtain thinner water blocking insulating layers. In addition, more experiments should be carried out to study the blocking capability of P4VP for HCl more thoroughly.
Finally, solutions of $CaCl_2$ and $MgCl_2$ should be applied to the PAA single-gate field-effect transistors to verify that they will not influence the transistor characteristics. Solutions of glucose have to be studied as well. Next, experiments should be carried out to determine the influence of buffer solutions with different pH.

## 5.3. A look ahead

When the aforementioned subjects are studied and thoroughly understood, the next steps can be taken on the way of measuring on neurons. Neurons need the right surface to properly adhere to and grow on, like surfaces consisting of poly-L-lysine or laminin. It has to be found out how to easily spincoat these layers on top of a single-gate field-effect transistor. Also the influence on the transistor characteristics has to be studied. Next, neurons need to be grown on top of the transistor and guided through the channels in the PDMS block. When neurons can be kept alive on top of the transistor, measurements can be performed on the neurons. Finally, the action potentials of the neuron can be measured by the field-effect transistor. Later, experiments can be carried out to also use the field-effect transistor to induce action potentials by stimulating the neurons. Meanwhile, work should also be done to replace the rigid silicon gate by a flexible organic material. When all of this has been done, a true plastic neuronal signal sensor will be obtained.

# 6. References


[1] K.V. Shenoy, G. Santhanam, S.I. Ryu, A. Afshar, B.M. Yu, V. Gilja, M.D. Linderman, R.S. Kalmar, J.P. Cunningham, C.T. Kemere, A.P. Batista, M.M. Churchland and T.H. Meng, *Increasing the performance of cortically-controlled prostheses*, Engineering in Medicine and Biology Society, 2006. EMBS '06. 28th Annual International Conference of the IEEE **Supplement**, 6652-6656 (2006)

[2] L.R. Hochberg and J.P. Donoghue, *Sensors for brain-computer interfaces*, IEEE Eng. Med. Biol. Mag. **25**, 32-38 (2006)

[3] M.D. Linderman, G. Santhanam, C.T. Kemere, V. Gilja, S. O'Driscoll, B.M. Yu, A. Afshar, S.I. Ryu, K.V. Shenoy and T.H. Meng, *Signal processing challenges for neural prostheses*, IEEE Signal Process Mag. **25**, 18-28 (2008)

[4] K. Cheung, *Implantable microscale neural interfaces*, Biomed. Microdevices **9**, 923-938 (2007)

[5] T. Sinkjaer, *Integrating sensory nerve signals into neural prosthesis devices*, Neuromodulation **3**, 34-41 (2000)

[6] B. Alberts, D. Bray, J. Lewis, M. Raff, K. Roberts and J.D. Watson, *Molecular biology of the cell, second edition*, Garland Publishing, Inc., 1306 pp. (1989)

[7] J. Darnell, H.F. Lodish and D. Baltimore, *Molecular cell biology, second edition*, Scientific American Books, Inc., 1147 pp. (1990)

[8] F.G. Donnan, *Theory of membrane equilibria and membrane potentials in the presence of non-dialysing electrolytes. A contribution to physical-chemical physiology*, J. Membr. Sci. **100**, 45-55 (1995)

[9] D.F. Shriver and P.W. Atkins, *Inorganic chemistry, third edition*, Oxford University Press, 786 pp. (2002)

[10] A.L. Hodgkin and B. Katz, *The effect of sodium ions on the electrical activity of the giant axon of the squid*, J. Physiol. **108**, 37-77 (1949)

[11] B.R. Eggins, *Biosensors, an introduction*, John Wiley and Teubner, 212 pp. (1996)

[12] D.G. Buerk, *Biosensors, theory and applications*, Technomic Publishing Company, 221 pp. (1993)

[13] A. Branner, R.B. Stein and R.A. Normann, *Selective stimulation of cat sciatic nerve using an array of varying-length microelectrodes*, J. Neurophysiol. **85**, 1585-1594 (2001)

[14] W.L.C. Rutten, *Selective electrical interfaces with the nervous system*, Annu. Rev. Biomed. Eng. **4**, 407-452 (2002)

[15] T. Stieglitz, M. Schuetter and K.P. Koch, *Implantable biomedical microsystems for neural prostheses*, IEEE Eng. Med. Biol. Mag. **24**, 58-65 (2005)

[16] A.S. Widge, M. Jeffries-El, X. Cui, C.F. Lagenaur and Y. Matsuoka, *Self-assembled monolayers of polythiophene conductive polymers improve biocompatibility and electrical impedance of neural electrodes*, Biosens. Bioelectron. **22**, 1723-1732 (2007)

[17] X. Cui and D.C. Martin, *Electrochemical deposition and characterization of poly(3,4-ethylenedioxythiophene) on neural microelectrode arrays*, Sens.

Actuators, B **89**, 92-102 (2003)
[18] K.C. Cheung, P. Renaud, H. Tanila and K. Djupsund, *Flexible polyimide microelectrode array for in vivo recordings and current source density analysis*, Biosens. Bioelectron. **22**, 1783-1790 (2007)
[19] T. Nyberg, O. Inganäs and H. Jerregård, *Polymer hydrogel microelectrodes for neural communication*, Biomed. Microdevices **4**, 43-52 (2002)
[20] E.J. Meijer, *Charge transport in disordered organic field-effect transistors*, PhD Thesis, Delft University of Technology, 143 pp. (2003)
[21] S.M. Sze, *Physics of semiconductor devices*, *second edition*, John Wiley & Sons, 868 pp. (1981)
[22] S. Iba, T. Sekitani, Y. Kato, T. Someya, H. Kawaguchi, M. Takamiya, T. Sakurai and S. Takagi, *Control of threshold voltage of organic field-effect transistors with double-gate structures*, Appl. Phys. Lett. **87**, 023509-3 (2005)
[23] M. Morana, G. Bret and C. Brabec, *Double-gate organic field-effect transistor*, Appl. Phys. Lett. **87**, 153511-3 (2005)
[24] J.B. Koo, K.S. Suh, I.K. You and S.H. Kim, *Device characteristics of pentacene dual-gate organic thin-film transistor*, Jpn. J. Appl. Phys. **46**, 5062-5066 (2007)
[25] G.H. Gelinck, E. van Veenendaal and R. Coehoorn, *Dual-gate organic thin-film transistors*, Appl. Phys. Lett. **87**, 073508-3 (2005)
[26] F. Maddalena, M. Spijkman, J.J. Brondijk, P. Fonteijn, F. Brouwer, J.C. Hummelen, D.M. de Leeuw, P.W.M. Blom and B. de Boer, *Device characteristics of polymer dual-gate field-effect transistors*, Org. Electron. (2008), doi:10.1016/ j.orgel.2008.06.004
[27] M. Merz and P. Fromherz, *Silicon chip interfaced with a geometrically defined net of snail neurons*, Adv. Funct. Mater. **15**, 739-744 (2005)
[28] A. Lambacher, M. Jenkner, M. Merz, B. Eversmann, R.A. Kaul, F. Hofmann, R. Thewes and P. Fromherz, *Electrical imaging of neuronal activity by multi-transistor-array (MTA) recording at 7.8 µm resolution*, Appl. Phys. A **79**, 1607-1611 (2004)
[29] A. Offenhäusser, C. Sprössler, M. Matsuzawa and W. Knoll, *Field-effect transistor array for monitoring electrical activity from mammalian neurons in culture*, Biosens. Bioelectron. **12**, 819-826 (1997)
[30] M. Voelker and P. Fromherz, *Signal transmission from individual mammalian nerve cell to field-effect transistor*, Small **1**, 206-210 (2005)
[31] F. Patolsky, B.P. Timko, G. Yu, Y. Fang, A.B. Greytak, G. Zheng and C.M. Lieber, *Detection, stimulation, and inhibition of neuronal signals with high-density nanowire transistor arrays*, Science **313**, 1100-1104 (2006)
[32] J.T. Mabeck and G.G. Malliaras, *Chemical and biological sensors based on organic thin-film transistors*, Anal. Bioanal. Chem. **384**, 343-353 (2006)
[33] G. Harsányi, *Polymer films in sensor applications: a review of present uses and future possibilities*, Sensor Review **20**, 98-105 (2000)
[34] R.R. Richardson, J.A. Miller and W.M. Reichert, *Polyimides as biomaterials: preliminary biocompatibility testing*, Biomaterials **14**, 627-635 (1993)
[35] G. Kotzar, M. Freas, P. Abel, A. Fleischman, S. Roy, C. Zorman, J.M. Moran and J. Melzak, *Evaluation of MEMS materials of construction for implantable medical*

*devices*, Biomaterials **23**, 2737-2750 (2002)
[36] E. Fournier, C. Passirani, C.N. Montero-Menei and J.P. Benoit, *Biocompatibility of implantable synthetic polymeric drug carriers: focus on brain biocompatibility*, Biomaterials **24**, 3311-3331 (2003)
[37] D. Feili, M. Schuettler, T. Doerge, S. Kammer and T. Stieglitz, *Encapsulation of organic field effect transistors for flexible biomedical microimplants*, Sens. Actuators, A **120**, 101-109 (2005)
[38] D. Feili, M. Schuettler and T. Stieglitz, *Matrix-addressable, active electrode arrays for neural stimulation using organic semiconductors—cytotoxicity and pilot experiments in vivo*, J. Neural Eng. **5**, 68-74 (2008)
[39] M. Deen and F. Pascal, *Electrical characterization of semiconductor materials and devices—review*, J. Mater. Sci.: Mater. Electron. **17**, 549-575 (2006)
[40] M. Heeney, C. Bailey, K. Genevicius, M. Shkunov, D. Sparrowe, S. Tierney and I. McCulloch, *Stable polythiophene semiconductors incorporating thieno[2,3-b]thiophene*, J. Am. Chem. Soc. **127**, 1078-1079 (2005)
[41] M.-H. Yoon, H. Yan, A. Facchetti and T.J. Marks, *Low-voltage organic field-effect transistors and inverters enabled by ultrathin cross-linked polymers as gate dielectrics*, J. Am. Chem. Soc. **127**, 10388-10395 (2005)
[42] Y.-Y. Noh, N. Zhao, M. Caironi and H. Sirringhaus, *Downscaling of self-aligned, all-printed polymer thin-film transistors*, Nat. Nanotechnol. **2**, 784-789 (2007)
[43] J. Veres, S. Ogier, G. Lloyd and D. de Leeuw, *Gate insulators in organic field-effect transistors*, Chem. Mater. **16**, 4543-4555 (2004)
[44] A. Facchetti, M.-H. Yoon and T.J. Marks, *Gate dielectrics for organic field-effect transistors: New opportunities for organic electronics*, Adv. Mater. **17**, 1705-1725 (2005)

# Euhh, wát heb je gedaan?!

## Een plastic transistor voor het meten van zenuwsignalen

“Vandaag heb ik de toekomst bezocht. Ik was op bezoek, thuis bij een jongen. Ik vertelde hem hoe ik in zijn tijd terecht was gekomen. Meteen liep hij naar zijn computer. Hij keek naar het scherm en bladerde door een aantal websites. Toen ik vroeg waar zijn muis en toetsenbord waren, keek hij me lachend aan. Zoiets was toch ouderwets? Hij tikte op zijn hoofd. ‘Hier. Hier zit het. Een chip meet mijn hersen- en zenuwsignalen. Zó bestuur ik mijn pc.’ Niks geen muis of toetsenbord dus.”

Zo zou het dagboek eruit kunnen zien van iemand die naar de toekomst kan reizen. Een toekomst waarin je niet meer een muis of toetsenbord gebruikt, maar de computer met je gedachten bestuurt. Op dit moment is zoiets nog sciencefiction, maar er wordt al veel onderzoek gedaan in deze richting. Dit onderzoek richt zich voorlopig vooral op toepassingen voor de medische wereld.
Eén van die toepassingen gaat bijvoorbeeld over het helpen van mensen met een dwarslaesie. Mensen met een dwarslaesie hebben een beschadiging opgelopen in hun ruggenmerg, vaak door een verkeersongeluk. Een dwarslaesie leidt er toe dat de zenuwsignalen van sommige delen van het lichaam niet meer de hersenen kunnen bereiken, en omgekeerd. Een bekend gevolg is verlamming van de benen of de armen. In sommige gevallen kan zelfs spraakverlies optreden.
Het onderzoek naar de dwarslaesie toepassing kijkt vooral naar manieren om de zenuwsignalen te meten in het niet-beschadigde deel van de zenuwen en het ruggenmerg. Deze signalen kunnen dan gebruikt worden om bijvoorbeeld een kunstbeen of spraakcomputer aan te sturen.

**Zenuwsignalen**
Alle medische toepassingen, maar ook de muisloze toekomstcomputer, hebben met elkaar gemeen dat ze op de één of andere manier de zenuwsignalen moeten meten.

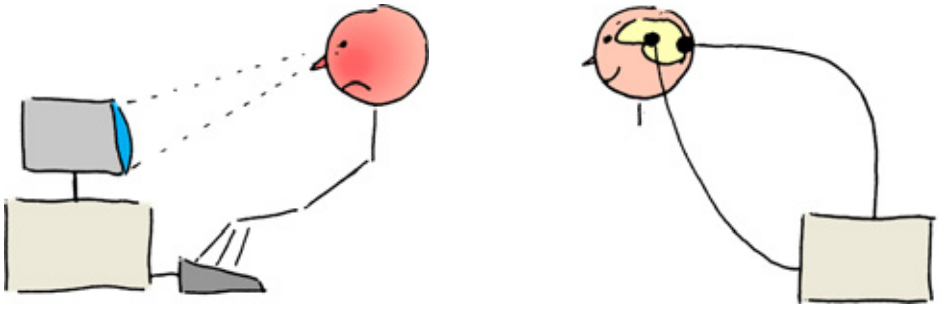

**Een toekomst zonder muis en toetsenbord.** *Een computer die je met je gedachten bestuurt, is nu nog sciencefiction. Tekening: P. Fromherz, ChemPhysChem* ***3****, 276-284 (2002).*

Maar wat zijn deze zenuwsignalen eigenlijk? Om dit te begrijpen moeten we kijken naar wat er gebeurt in een zenuwcel. In een zenuwcel zitten een heleboel stoffen die belangrijk zijn voor de cel om te overleven. De belangrijkste hiervan voor de zenuwsignalen zijn ionen. Een ion is een atoom of molecuul met een elektrische lading. Deze lading kan positief (+) of negatief (−) zijn. Sommige ionen kunnen door de wand van de zenuwcel naar binnen of naar buiten lekken. De binnenkant van de zenuwcel krijgt hierdoor een negatieve lading. De buitenkant van de zenuwcel wordt daardoor positief geladen.
Deze ladingen veranderen als een zenuwcel geprikkeld wordt. Op de plek van de prikkeling gaan er kanaaltjes open in de wand van de zenuwcel. Op deze plek stromen er nu een heleboel extra ionen de zenuwcel binnen. Hierdoor krijgt de binnenkant van dit stukje zenuwcel ineens een positieve lading en de buitenkant een negatieve lading. Deze verandering van de ladingen is het zenuwsignaal.
De verandering van de ladingen op de plek van de prikkeling zorgt er voor dat de kanaaltjes in het naastgelegen stukje van de zenuwcel ook open gaan. Hierdoor veranderen de ladingen in dat stukje zenuwcel dus ook. Daardoor gaan ook de verderop gelegen kanaaltjes open, waardoor daar ook de ladingen veranderen. Zo beweegt het zenuwsignaal als een soort elektrisch stroompje langs de zenuwcel.

**Transistors**
Een zenuwsignaal is een erg zwak signaal. Bovendien duurt een zenuwsignaal erg kort. Al na 1 milliseconde (een duizendste van een seconde) zijn de ladingen veranderd. Om een zenuwsignaal te meten, moet je dus heel gevoelig en heel snel kunnen meten. Dit kan door gebruik te maken van een transistor.
Een transistor is een soort aan-uit schakelaar. Transistors worden veel gebruikt in allerlei elektrische apparaten. Zo bestaat bijvoorbeeld een computer processor uit miljoenen transistors. Een transistor wordt gemaakt van een halfgeleider materiaal. Een halfgeleider kan een elektrische stroom geleiden. In een transistor gebeurt dit alleen in bepaalde omstandigheden. Of een transistor stroom geleidt, hangt af van de ladingen die op de transistor zitten. Als de transistor stroom geleidt, dan zeggen we dat de transistor ‘aan’ is. Als er geen stroom loopt, dan is de transistor ‘uit’. Door de ladingen op de transistor te veranderen, kan de transistor aan- en uitgezet worden, net als een schakelaar. Vaak is een klein verschil in ladingen al genoeg om de

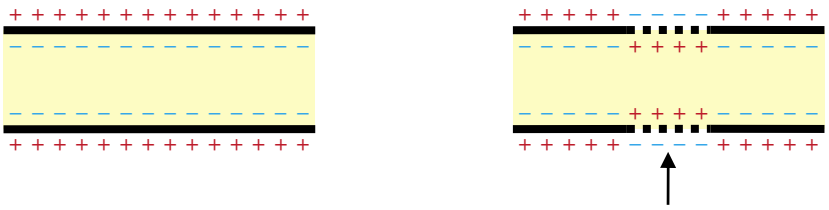

**Een zenuwsignaal op een stukje van een zenuwcel.** *Normaal is de buitenkant van een zenuwcel positief geladen (links). Als de zenuwcel geprikkeld wordt (pijltje), veranderen de ladingen. De buitenkant van dit stukje zenuwcel wordt nu negatief (rechts).*

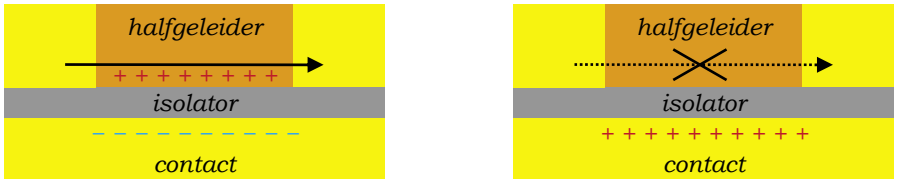


**Een transistor kun je aan- en uitzetten.** *Als er negatieve ladingen op de transistor zitten, dan geleidt de transistor stroom (links). De transistor is nu 'aan'. Als er positieve ladingen op de transistor zitten, dan loopt er geen stroom meer en is de transistor 'uit' (rechts). Voor sommige transistors is dit precies omgekeerd. Dit hangt af van de halfgeleider die je gebruikt.*

transistor aan- of uit te zetten. Een transistor kan daarom heel gevoelig gemaakt worden.
Zoals eerder beschreven, heeft een zenuwsignaal alles te maken met ladingen. De ladingen op een zenuwcel kunnen een transistor ook aan- of uitzetten. Hiervoor moet de zenuwcel natuurlijk wel tegen de transistor liggen. Als je nu de stroom door de transistor meet, weet je precies of en wanneer er een zenuwsignaal langs komt.

**Afweerreactie**
Er zijn al een aantal onderzoekers die een zenuwcel op een transistor hebben laten groeien. Zij konden inderdaad zenuwsignalen meten. Alle onderzoekers gebruikten silicium als de halfgeleider in hun transistors. Silicium wordt ook gebruikt voor de transistors in een computer processor.
Een nadeel van silicium is dat het een lichaamsvreemd materiaal is. Bovendien is het niet erg flexibel en dus niet gemakkelijk te buigen. Als een silicium transistor in je lichaam wordt geïmplanteerd, dan ontstaan er ontstekingen en afweerreacties. Hierdoor werkt de transistor minder goed. De ontstekingen en afweerreacties kunnen er echter ook voor zorgen dat je zenuwcellen beschadigd raken.
Om het ontstaan van ontstekingen en afweerreacties te voorkomen, is het beter om een andere halfgeleider dan silicium te gebruiken. Een goed alternatief zijn organische polymeren, een soort van plastics. Een polymeer is een lang molecuul opgebouwd uit een heleboel aan elkaar gekoppelde kortere stukjes. Je kunt het vergelijken met een lange kralenketting. Polymeren zijn daardoor erg flexibel.
Sommige organische polymeren kunnen een beetje stroom geleiden en zijn net als silicium een halfgeleider. Bovendien kun je ze zo ontwerpen dat ze in je lichaam veel minder ontstekingen en afweerreacties opwekken. Polymeren zijn dus heel geschikt om te gebruiken in een transistor voor het meten van zenuwsignalen.

**Mijn onderzoek**
Het afgelopen jaar heb ik mijn master onderzoeksproject gedaan in de onderzoekgroep *Molecular Electronics - Physics of Organic Semiconductors*. De onderzoekers in deze groep hebben veel ervaring met organische polymeren. Ze gebruiken halfgeleidende organische polymeren om bijvoorbeeld plastic LED lampen, plastic zonnecellen en

plastic transistors te maken. In mijn onderzoek heb ik gekeken of je deze plastic transistors uiteindelijk misschien ook kunt gebruiken om zenuwsignalen te meten.

**Water**

Zenuwcellen kunnen alleen overleven in een waterige omgeving, net als in je lichaam. Je kunt echter problemen krijgen als je een transistor in water stopt. De stroom in een transistor is vaak zo groot dat watermoleculen uit elkaar vallen. Er ontstaan dan allemaal belletjes van waterstof en zuurstof. Dit is zo'n heftige reactie dat de transistor er stuk van gaat.

Het is dus belangrijk om de transistor te beschermen. Daarom ben ik in mijn onderzoek op zoek gegaan naar een beschermlaag die water tegen kan houden. Het lukte om een goede beschermlaag te maken van polymethylmethacrylaat (PMMA). PMMA is ook wel bekend als plexiglas en is een isolerend polymeer. Het bleek dat een laag van 1000 nm dik PMMA water goed kon tegenhouden (1 nm is een miljardste van een meter). Voor een transistor is dit helaas een heel dikke laag. Met zo'n dikke beschermlaag op de transistor zijn er ontzettend veel ladingen nodig om de transistor aan- en uit te zetten. Een zenuwsignaal heeft hier te weinig ladingen voor. Om de transistor toch aan- en uit te zetten met een zenuwsignaal moet de beschermlaag dus nog dunner zijn.

***Crosslinker***

Op het niveau van de moleculen is PMMA te vergelijken met een grote hoop kralenkettingen of spaghetti slierten. Voor een watermolecuul is er genoeg ruimte om tussen de moleculen door te glippen. Om water goed tegen te houden, moeten de polymeer moleculen een veel dichter netwerk vormen. Dit kun je voor elkaar krijgen door een *crosslinker* aan het polymeer toe te voegen. Een *crosslinker* is een stof die met het polymeer kan reageren. Het knoopt de polymeer moleculen als het ware aan elkaar vast. Zo ontstaat een veel dichter netwerk. Dankzij zo'n crosslinker was een laag PMMA van 500 nm dik al genoeg om water goed tegen te houden.

Door de *crosslinker* ontstond helaas een ander probleem. Bij de reactie van de *crosslinker* met PMMA werd een ion gevormd. Dit ion reageerde met het halfgeleider polymeer. Hierdoor kwamen er heel veel extra positieve ladingen in de halfgeleider, waardoor de transistor veel makkelijker stroom geleidde. Het was daardoor niet meer

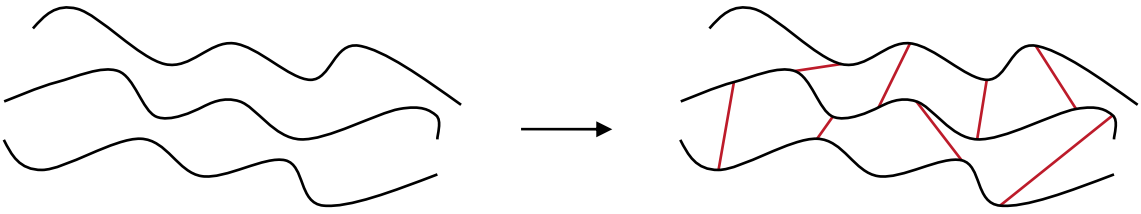

**Een polymeer met *crosslinker*.** *Een crosslinker (rood) knoopt de losse polymeer moleculen (zwart) aan elkaar vast. Daardoor ontstaat een veel dichter netwerk.*

mogelijk om de transistor aan- en uit te zetten.
Om dit probleem op te lossen, ben ik op zoek gegaan naar een extra beschermlaag die dit ion tegen kon houden. Het lukte om bovenop de halfgeleider een redelijk goede beschermlaag te maken. Deze laag werkte als een soort vangnet voor het ion, zodat het ion niet met de halfgeleider kon reageren. Dankzij deze extra beschermlaag bleef de transistor gewoon werken en kon toch de *crosslinker* gebruikt worden.

**Zoutoplossingen**
Zenuwcellen hebben niet alleen water nodig om te overleven. Ze hebben ook bepaalde zouten nodig, zoals natrium chloride (ook wel bekend als keukenzout) en kalium chloride (een onderdeel van dieetzout). Het is belangrijk om te weten wat de invloed is van deze zouten op de transistor. Als de zouten de transistor al aan- of uitzetten, dan kan de transistor niet meer gebruikt worden om zenuwsignalen te meten. Daarom heb ik in mijn onderzoek ook gekeken naar wat er gebeurt als je zoutoplossingen op de transistor legt. Zoals verwacht, beïnvloedden de zoutoplossingen de transistor helemaal niet. In een zoutoplossing zitten namelijk evenveel positieve- als negatieve ionen. De totale lading van een zoutoplossing is dus nul. Een zoutoplossing kan een transistor dus niet aan- of uitzetten en beïnvloedt een transistor dus niet.

Uit de resultaten van mijn onderzoek blijkt dat een plastic transistor geschikt is om uiteindelijk zenuwsignalen te meten. Er moeten echter nog heel veel dingen onderzocht worden voordat zo'n transistor echt gebruikt kan worden om zenuwsignalen te meten. Zo moeten allerlei andere stoffen getest worden of ze de transistor niet beïnvloeden. Ook is het beter om de beschermlaag tegen water nog dunner te maken. Daarna kan bekeken worden hoe je een zenuwcel op een plastic transistor moet laten groeien en in leven moet houden. Als dat lukt, kan er aan zenuwcellen gemeten gaan worden. Het duurt zeker nog tientallen jaren voordat je een plastic transistor echt kunt gebruiken om zenuwsignalen te meten in allerlei (medische) toepassingen. Tot die tijd moet je dus gewoon je muis en toetsenbord blijven gebruiken.